Stem Cell Reports
Article

ISSCR

OPEN ACCESS

H3K9 Demethylases JMJD1A and JMJD1B Control Prospermatogonia to Spermatogonia Transition in Mouse Germline

Shunsuke Kuroki,[1] Ryo Maeda,[1] Masashi Yano,[2] Satsuki Kitano,[3] Hitoshi Miyachi,[3] Mikiko Fukuda,[4] Yoichi Shinkai,[5] and Makoto Tachibana[1,2,*]

[1]Graduate School of Frontier Biosciences, Osaka University, 1-3 Yamadaoka, Suita, Osaka 565-0871, Japan
[2]Institute of Advanced Medical Sciences, Tokushima University, 3-18-15 Kuramoto-cho, Tokushima, Tokushima 770-8503, Japan
[3]Experimental Research Center for Infectious Diseases, Institute for Virus Research, Kyoto University, 53 Shogoin, Kawara-cho, Sakyo-ku, Kyoto, Kyoto 606-8597, Japan
[4]Center for iPS Cell Research and Application, Kyoto University, 53 Shogoin, Kawara-cho, Sakyo-ku, Kyoto, Kyoto 606-8597, Japan
[5]Cellular Memory Laboratory, Cluster for Pioneering Research, RIKEN, 2-1 Hirosawa, Wako, Saitama 351-0198, Japan
*Correspondence: tachiban@fbs.osaka-u.ac.jp
https://doi.org/10.1016/j.stemcr.2020.06.013

SUMMARY

Histone H3 lysine 9 (H3K9) methylation is dynamically regulated by methyltransferases and demethylases. In spermatogenesis, prospermatogonia differentiate into differentiating or undifferentiated spermatogonia after birth. However, the epigenetic regulation of prospermatogonia to spermatogonia transition is largely unknown. We found that perinatal prospermatogonia have extremely low levels of di-methylated H3K9 (H3K9me2) and that H3K9 demethylases, JMJD1A and JMJD1B, catalyze H3K9me2 demethylation in perinatal prospermatogonia. Depletion of JMJD1A and JMJD1B in the embryonic germline resulted in complete loss of male germ cells after puberty, indicating that H3K9me2 demethylation is essential for male germline maintenance. JMJD1A/JMJD1B-depleted germ cells were unable to differentiate into functional spermatogonia. JMJD1 isozymes contributed to activation of several spermatogonial stem cell maintenance genes through H3K9 demethylation during the prospermatogonia to spermatogonia transition, which we propose is key for spermatogonia development. In summary, JMJD1A/JMJD1B-mediated H3K9me2 demethylation promotes prospermatogonia to differentiate into functional spermatogonia by establishing proper gene expression profiles.

INTRODUCTION

Developmental gene expression is tuned by transcription factors and the levels of post-translational modifications. Covalent modifications of the core histone tail are important epigenetic marks linked to a wide variety of nuclear functions, including transcriptional regulation. The discovery of enzymes that add/remove methyl groups to/from histones suggests that histone methylation levels are not static but are dynamically regulated by a variety of processes (Kooistra and Helin, 2012). Histone H3 lysine 9 (H3K9) methylation, a representative epigenetic mark of transcriptionally silenced heterochromatin, is dynamically regulated by H3K9 methyltransferases and demethylases.

Spermatogenesis is a highly coordinated differentiation process in male germ cells. Dynamic regulation of H3K9 methylation plays a crucial role in spermatogenesis. Mice lacking H3K9 tri-methyltransferases, Suv39h1 and Suv39h2, displayed male germ cell arrest at the mid-to-late pachytene stage of meiosis (Peters et al., 2001). The germline-specific depletion of G9a, which catalyzes H3K9 di-methylation, resulted in early pachytene stage arrest in the male and female germline (Tachibana et al., 2007). Germline-specific depletion of H3K9 tri-methyltransferase, Eset, caused postnatal hypogonadism in both sexes (Liu et al., 2014). Finally, loss of H3K9 demethylase, JMJD1A, impeded spermatid elongation (Okada et al., 2007) (Liu et al., 2010).

Prospermatogonia are male germ cells located in the center of testis cords in the pre- and perinatal period. After birth, prospermatogonia differentiate into undifferentiated- or differentiating spermatogonia (de Rooij, 1998; Yoshida et al., 2006). How epigenetic regulation contributes to prospermatogonia to spermatogonia transition is largely unknown. We previously revealed that H3K9me2 in embryonic prospermatogonia is maintained at extremely low levels compared with somatic cells (Deguchi et al., 2013). We proposed that a low abundance of GLP/G9a heteromeric complex, a primary enzyme for H3K9 di-methylation (Tachibana et al., 2002, 2005), might partly account for H3K9me2 hypomethylation in prospermatogonia (Deguchi et al., 2013). However, contribution of H3K9 demethylase(s) to H3K9me2 hypomethylation was not determined.

Here, we show that H3K9me2 hypomethylation is maintained in postnatal prospermatogonia. We also show that H3K9me2 hypomethylation is achieved enzymatically via JMJD1A and JMJD1B, the enzymes responsible for H3K9me2 demethylation. We established a mouse line in which JMJD1A and/or JMJD1B were depleted in a germline-specific manner. Depletion of JMJD1A and JMJD1B resulted in a complete loss of male germ cells after puberty. Cytological analysis revealed that JMJD1A/JMJD1B-depleted germ cells could not differentiate into functional spermatogonia. Furthermore, transcriptome analysis

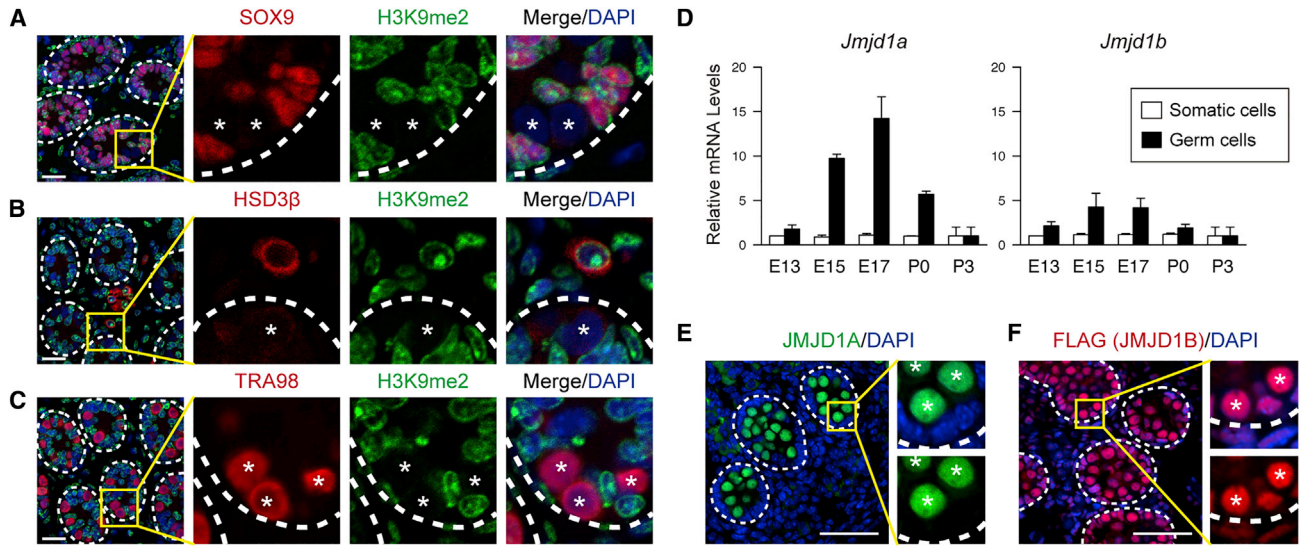

Figure 1. Expression Profiles of JMJD1A and JMJD1B in Prospermatogonia

(A–C) P3 wild-type mouse testes sections stained with an anti-H3K9me2 antibody. Sertoli cells and Leydig cells were marked with antibodies against SOX9 (A) and HSD3β (B), respectively. A TRA98 antibody was used to detect germ cells (C). Nuclei were stained with DAPI. Dashed lines represent basement membranes. Asterisks represent germ cells. Scale bars, 20 μm.

(D) Quantitative mRNA analysis for *Jmjd1a* (left) and *Jmjd1b* (right) in germ cells and somatic cells separated from *Oct4-EGFP* Tg testes at the indicated time points. Relative mRNA levels in E13.5 somatic cells were arbitrarily defined as 1. Data are presented as the mean ± SD (n = 3 mice for each time point).

(E and F) Immunofluorescence analysis of JMJD1A and JMJD1B in embryonic testes sections. Dashed lines represent basement membranes. Asterisks represent germ cells. Scale bars, 50 μm. (E) E17.5 wild-type testis sections were stained with an anti-JMJD1A antibody and DAPI. Enlarged boxes represent double staining for JMJD1A and DAPI (top) and single staining for JMJD1A (bottom). (F) E17.5 *Jmjd1b*$^{+/FLAG-KI}$ testes were stained with an anti-FLAG antibody and DAPI. Enlarged boxes represent double staining for FLAG and DAPI (top) and single staining for FLAG (bottom).

indicated that JMJD1A/JMJD1B-depleted germ cells did not undergo a change in gene expression from prospermatogonia to spermatogonia. Finally, we demonstrated that activation of serial spermatogonial stem cell (SSC) maintenance genes was dependent upon JMJD1-mediated H3K9 demethylation. In summary, we demonstrate the pivotal role of H3K9 demethylation in spermatogenesis, where JMJD1 isozymes promote the differentiation of prospermatogonia into functional spermatogonia.

RESULTS

Expression Profiles of JMJD1A and JMJD1B in Prospermatogonia

We previously demonstrated that H3K9me2 levels were significantly lower in prenatal prospermatogonia than in somatic cells during mouse embryogenesis (Deguchi et al., 2013). To examine whether H3K9me2 hypomethylation was maintained in postnatal prospermatogonia, we performed immunostaining for H3K9me2 on testis sections at postnatal day 3 (P3). Sections were stained with antibodies against SOX9 and HSD3b, markers for Sertoli cells and Leydig cells, respectively. Male germ cells were stained with a TRA98 antibody, which recognizes a mouse testicular germ cell-specific antigen (Tanaka et al., 1997). H3K9me2 signals were abundantly detected in the nuclei of Sertoli cells and Leydig cells in postnatal testes (Figures 1A and 1B, respectively). In contrast, H3K9me2 signals of prospermatogonia were extremely low, indicating that H3K9me2 hypomethylation was maintained from prenatal to postnatal prospermatogonia (Figure 1C).

We previously demonstrated that H3K9me2 hypomethylation in embryonic prospermatogonia was associated with reduced expression of GLP, a regulatory subunit of the GLP/G9a H3K9 methyltransferase complex (Deguchi et al., 2013; Tachibana et al., 2005; Ueda et al., 2006). Introduction of a *GLP* transgene increased H3K9me2 in prospermatogonia. However, the H3K9me2 levels were still lower than in somatic cells in this transgenic line (Deguchi et al., 2013). One explanation for this observation is that H3K9me2 demethylation machinery also functions in prospermatogonia. The Jmjd1 family of proteins, JMJD1A and JMJD1B, possess intrinsic H3K9 demethylating activity

and are involved in transcriptional activation (Yamane et al., 2006). We recently demonstrated the redundant but essential function of JMJD1A and JMJD1B in the peri-implantation stage of embryogenesis (Kuroki et al., 2018). To address the potential contribution of JMJD1A and JMJD1B to H3K9me2 hypomethylation in prospermatogonia, male germ cells were isolated from prenatal and postnatal testes for mRNA analysis. qRT-PCR analysis revealed that *Jmjd1a* mRNA was expressed more highly in germ cells than in somatic cells from embryonic day 15.5 (E15.5) to P3 (Figure 1D, left). Of note, *Jmjd1a* expression in prospermatogonia increased during late embryogenesis, reaching a peak at E17.5. Furthermore, prospermatogonia expressed higher levels of *Jmjd1b* mRNA compared with somatic cells, with peak expression at E15.5 (Figure 1D, right). Immunofluorescence analysis of E17.5 sections indicated that JMJD1A signals were abundant in germ cells but not in somatic cells (Figure 1E) consistent with the mRNA expression analyses (Figure 1D, left). To detect the endogenous JMJD1B protein, we established a knockin mouse carrying the $Jmjd1b^{FLAG-KI}$ allele, which produced a JMJD1B protein with a C-terminal FLAG tag (Kuroki et al., 2018). JMJD1B-FLAG was detected both in germ and somatic cells, but the levels of JMJD1B-FLAG were substantially higher in germ cells compared with somatic cells (Figure 1F) consistent with the mRNA analyses (Figure 1D, right). In summary, expression profiles of JMJD1A and JMJD1B do not contradict our hypothesis that JMJD1 isozymes might contribute to active H3K9me2 demethylation in prospermatogonia.

JMJD1A and JMJD1B Catalyze H3K9 Demethylation in Prospermatogonia

To address the role of JMJD1 isozymes in H3K9me2 hypomethylation in the male germline, we performed loss-of-function analyses of JMJD1A and/or JMJD1B. The combined loss of JMJD1A and JMJD1B led to lethality in the early post-implantation period (Kuroki et al., 2018); therefore, we generated mice in which *Jmjd1a* and *Jmjd1b* were conditionally deleted by Cre-*loxP*-mediated recombination. The *loxP*-flanked (2lox) conditional alleles of *Jmjd1a* and *Jmjd1b* are shown in Figure S1A and are described in our previous report (Kuroki et al., 2018). Mice carrying 2lox alleles of *Jmjd1a* and *Jmjd1b* were crossed with *Vasa-Cre* mice, to produce progeny in which Cre/*loxP*-mediated recombination occurs in germ cells from E15 (Gallardo et al., 2007). To address the accuracy of cell-type-specific depletion of JMJD1A and JMJD1B, germ cells were isolated from neonatal testes for immunoblot analysis. JMJD1A and JMJD1B were not detected in *Vasa-Cre*; $Jmjd1a^{2lox/1lox}$; $Jmjd1b^{2lox/1lox}$ germ cells, but were abundant in control *Vasa-Cre*; $Jmjd1a^{+/1lox}$; $Jmjd1b^{+/1lox}$ germ cells (Figures 2A and 2B). Importantly, in somatic cells, JMJD1B was still detected in *Vasa-Cre*; $Jmjd1a^{2lox/1lox}$; $Jmjd1b^{2lox/1lox}$ mice at a similar level to that in control mice (Figure 2B). These data indicate that JMJD1 isozymes were successfully depleted before birth in a germ cell-specific manner.

To address the potential contribution of JMJD1A and JMJD1B to H3K9me2 hypomethylation in prospermatogonia, we examined H3K9me2 in *Jmjd1a* and *Jmjd1b* mutant testes at P3. A schematic illustration of the generation of serial mutant mice is shown in Figure S1B. We hereafter describe the genotype of germ cells in *Vasa-Cre*; $Jmjd1a^{2lox/+}$; $Jmjd1b^{2lox/+}$ mice as *1a*Δ/+; *1b*Δ/+. Anti-H3K9me2 immunofluorescence analysis revealed that H3K9me2 in *1a*Δ/Δ; *1b*Δ/+ cells and *1a*Δ/+; *1b*Δ/Δ cells was significantly increased compared with that in *1a*Δ/+; *1b*Δ/+ cells (Figure 2C and summarized in Figure 2D). Notably, H3K9me2 was profoundly increased by the *1a*Δ/Δ mutation and moderately increased by the *1b*Δ/Δ mutation, indicating the predominant role of JMJD1A in H3K9me2 demethylation in prospermatogonia. Remarkably, the *1a*Δ/Δ; *1b*Δ/Δ mutation induced a >6-fold increase in H3K9me2 compared with that in the *1a*Δ/+; *1b*Δ/+ control (Figures 2C and 2D). H3K9me3 but not H3K9me1 was also increased in *1a*Δ/Δ; *1b*Δ/Δ male germ cells (Figures S2A and S2B, respectively). These data indicate that JMJD1A and JMJD1B preferentially demethylate H3K9me2/3 but not me1 in prospermatogonia. An *in vitro* enzymatic study demonstrated that recombinant JMJD1A demethylates H3K9me1/2, but not me3 (Yamane et al., 2006). It is reasonable that specific partner protein(s) may alter the substrate specificity of JMJD1 enzymes *in vivo*.

JMJD1A and JMJD1B Are Required for Maintenance of the Male Germline

To address the impact of JMJD1A/JMJD1B depletion on spermatogenesis, we performed histological analysis of reproductive organs in 3-month-old male mice (Figures 3A–3F) and summarized the number of germ cells per seminiferous tubule section (Figure 3G). Spermatogenesis in *1a*Δ/+; *1b*Δ/+ and *1a*+/+; *1b*Δ/Δ germ cells proceeded normally (Figures 3A and 3B). *1a*Δ/+; *1b*Δ/Δ germ cells could also differentiate into mature sperm, but populations of spermatids were moderately decreased compared with those in *1a*Δ/+; *1b*Δ/+ and *1a*+/+; *1b*Δ/Δ cells (Figures 3C and 3G). Male mice of these three mutants were fertile in natural mating. In contrast, a single homozygous mutation in *Jmjd1a* (*1a*Δ/Δ; 1b+/+) resulted in failure of the elongation step of spermiogenesis and the corresponding male mice were infertile (Figure 3D), indicating that JMJD1A is required for spermiogenesis. Previous reports demonstrated that the zygotic loss of JMJD1A results in failure of the elongation step of spermiogenesis (Liu et al., 2010; Okada et al., 2007). Taken together, our conditional

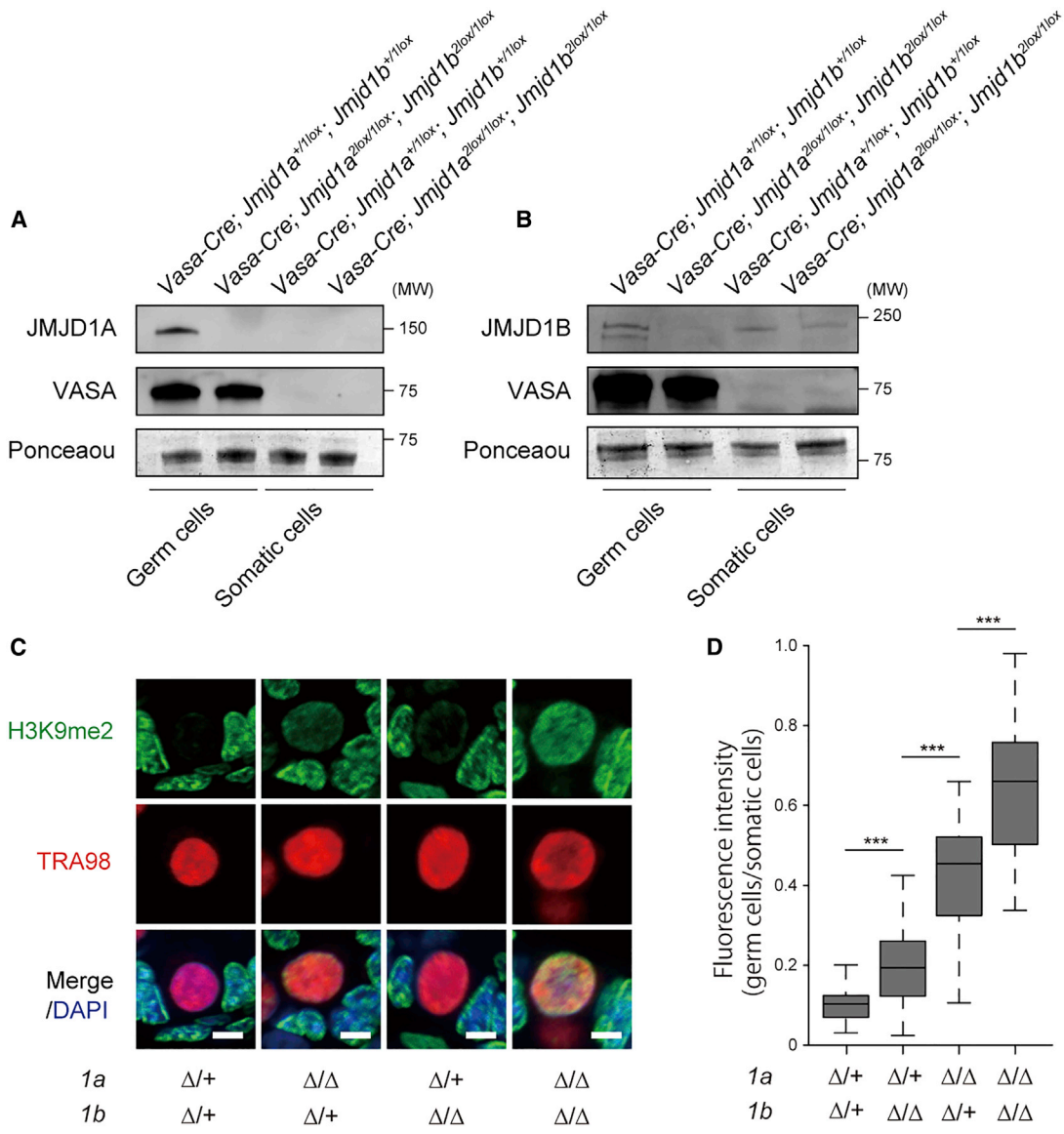

Figure 2. JMJD1A and JMJD1B Catalyze H3K9me2 Demethylation in Prospermatogonia

(A and B) Immunoblot analysis of JMJD1A (A) and JMJD1B (B) in neonatal testicular cells. Germ cells and somatic sells were separated from P0 testes of the indicated genotypes for immunoblot analysis. Enrichment of germ cells was confirmed by immunoblotting with an anti-VASA antibody. Ponceau staining was used as a loading control.

(C) Immunofluorescence analysis of H3K9me2 in P3 testes sections from the indicated genotypes. A TRA98 antibody was used to detect germ cells. Scale bars, 5 μm.

(D) Relative fluorescence intensities of H3K9me2 in P3 germ cells of the indicated genotypes. Fluorescence intensities of germ cells and neighboring Sertoli cells were measured using ImageJ software. Relative fluorescence intensity values were calculated by dividing the fluorescence intensities of germ cells by those of Sertoli cells. We examined >50 germ cells per genotype. ***$p < 0.001$ (one-way ANOVA with Tukey's test).

knockout studies confirmed that the spermiogenesis defect in JMJD1A-deficient mice was caused by a malfunction in the germ cell itself. Importantly, an additional 1b mutation on the *1a*Δ/Δ background had a profound effect on spermatogenesis (Figures 3E and 3G). Haploid spermatids were barely detected in testes carrying *1a*Δ/Δ; *1b*Δ/+ germ cells, suggesting that meiosis was perturbed in this mutant. Consistent with this, haploid germ cells were markedly reduced in adult testis carrying *1a*Δ/Δ; *1b*Δ/+ germ cells (Figure S3). These results indicate that JMJD1 isozymes

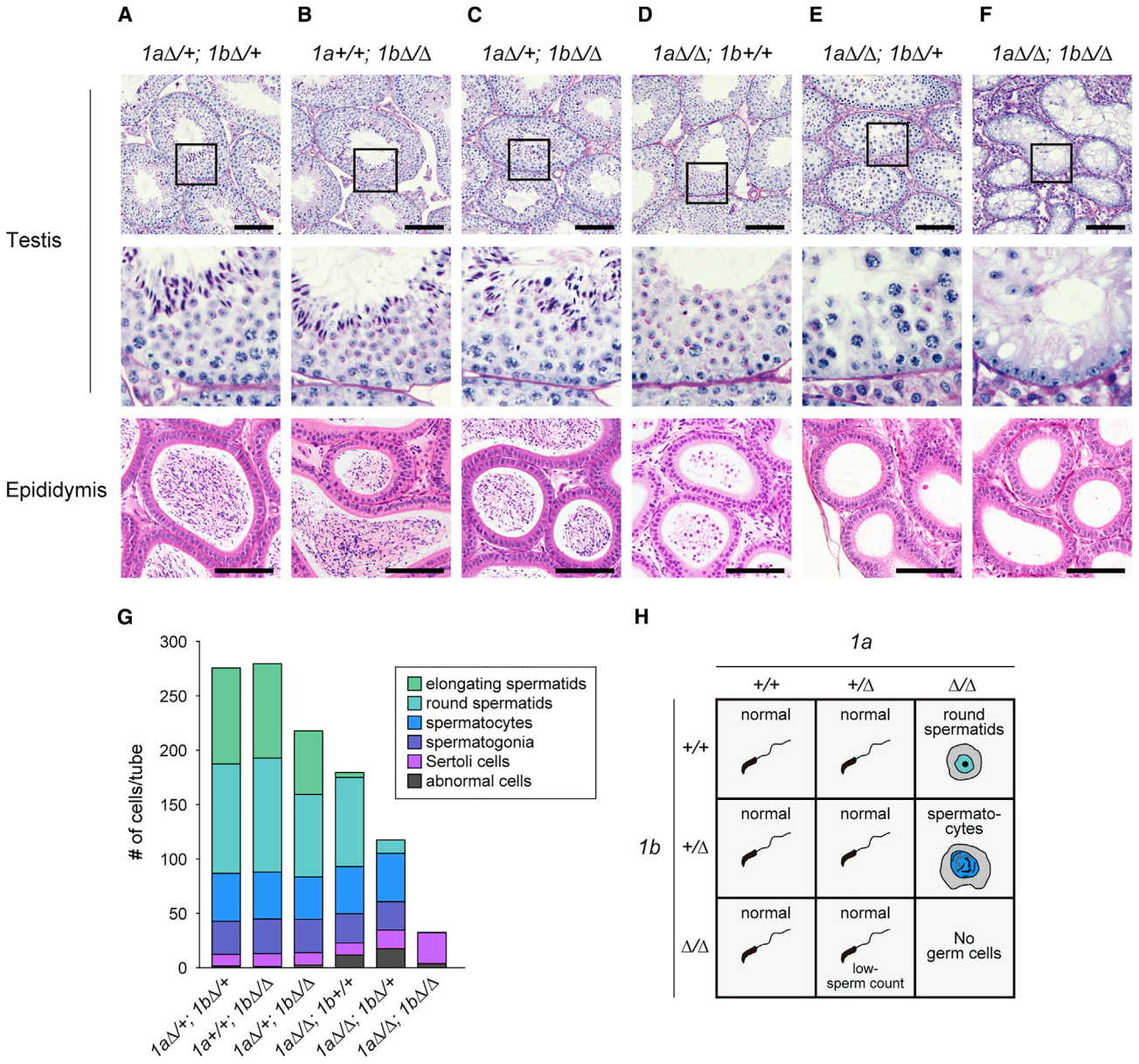

Figure 3. JMJD1A and JMJD1B Are Required for Maintenance of the Male Germline

(A–F) Histological analysis of testes and epididymis of 3-month-old male mice of the genotypes indicated above each figure (A) to (F). Paraffin-embedded testis and epididymis sections were stained with PAS-hematoxylin and hematoxylin-eosin, respectively. Enlarged views of testes sections (boxed areas in the top panel) are shown in the middle panel. Scale bars, 100 μm.

(G) Population analysis of testicular cells in 3-month-old testes of the indicated genotypes. The number of cells per PAS-hematoxylin-stained cross-tubular section is presented. Testicular cells were classified into six types according to their PAS-hematoxylin-staining profile, morphology, and intratubular localization. Abnormal cells represent those that could not be classified. More than 10 tubular sections were analyzed per sample.

(H) Summary of the developmental phenotypes of male germ cells lacking *Jmjd1a* and/or *Jmjd1b* alleles. Terminal developmental stages of male germ cells of the indicated genotypes are illustrated.

may play a crucial role in meiosis progression. Most importantly, loss of all *Jmjd1a* and *Jmjd1b* alleles resulted in the absence of germ cells at any developmental stage; only Sertoli cells were present in the corresponding seminiferous tubules of adult mice (Figures 3F and 3G). The final developmental stages of spermatogenesis in each mutant are

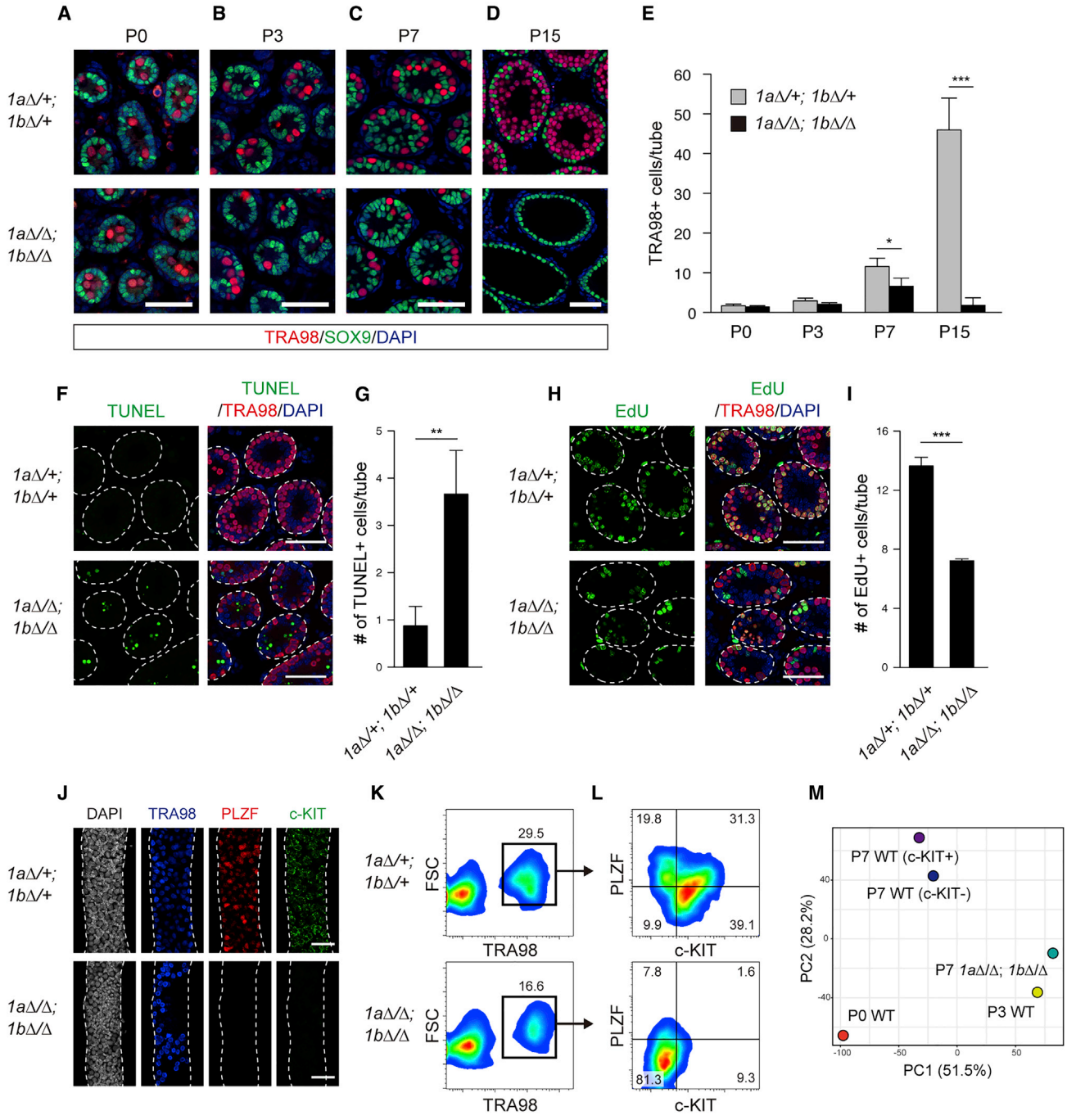

Figure 4. Germline-Specific Depletion of JMJD1A and JMJD1B Impairs Spermatogonia Development

(A–D) Immunofluorescence analysis of control (*1a*Δ/+; *1b*Δ/+, top) and mutant (*1a*Δ/Δ; *1b*Δ/Δ, bottom) testes sections at the developmental times indicated above each figure (A) to (D). Germ cells and Sertoli cells were marked with TRA98 and anti-SOX9 antibodies, respectively. Scale bars, 50 μm.

(E) Summarized number of TRA98+ germ cells per cross-tubular section at the indicated times. Error bars represent ± SEM for >100 tubules from three mice. ***p < 0.001 (t test).

(F–I) Cell death and proliferation analyses of JMJD1A/JMJD1B-depleted germ cells at P7. (F) TUNEL-stained sections of P7 testes of the indicated genotypes were counterstained with a TRA98 antibody and DAPI. Scale bars, 50 μm. (G) Average numbers of TUNEL+ cells in cross-tubular sections are summarized. Error bars represent ± SEM (n = 3 mice each). **p < 0.05 (t test). (H) P7 testicular cells

(legend continued on next page)

summarized in Figure 3H. We found redundant but partially different roles of *Jmjd1* alleles in spermatogenesis. First, at least one allele of either *Jmjd1a* or *Jmjd1b* is required for the maintenance of germ cells. Second, at least one allele of *Jmjd1a* or two alleles of *Jmjd1b* is required for the completion of meiosis. Third, at least one allele of *Jmjd1a* is required for the completion of the elongation step. In the latter two cases, the *Jmjd1a* allele is more important than the *Jmjd1b* allele.

Germline-Specific Depletion of JMJD1A and JMJD1B Impairs Spermatogonia Development

To identify the critical step of germ cell development influenced by JMJD1A/JMJD1B depletion, we examined when germ cells are exhausted in the mutant testes (Figures 4A–4D). Immunohistochemical analysis revealed that germ cells were barely detected in mutant testes at P15, in which only SOX9+ Sertoli cells were detected (Figure 4D). This indicated that *1a*Δ/Δ; *1b*Δ/Δ germ cells do not enter first-round spermatogenesis. In contrast, germ cells were detected in mutant testes until P7 (Figures 4A–4C). We counted germ cells per tubule of the mutant testes, as summarized in Figure 4E. No significant reduction was observed in the number of germ cells in mutant testes from P0 to P3. However, the number of germ cells was reduced in mutant testis at P7 (Figures 4C and 4E). Because spermatogonia are the dominant population in normal testes at P7, spermatogonia development may be influenced by JMJD1A/JMJD1B depletion. To address the cause of the reduction in germ cell number, we performed cell death and proliferation analyses of mutant testes at P7 (Figures 4F–4I). The number of apoptotic cells was markedly increased in testes carrying *1a*Δ/Δ; *1b*Δ/Δ germ cells (Figures 4F and 4G). 5-Ethynyl-2′-deoxyuridine (EdU) incorporation analysis indicated that proliferation was also affected in *1a*Δ/Δ; *1b*Δ/Δ germ cells (Figures 4H and 4I). We therefore concluded that an increase in cell death and a decrease in cell proliferation both account for the reduced number of *1a*Δ/Δ; *1b*Δ/Δ germ cells.

Spermatogonia are classified as two cell types, differentiating and undifferentiated spermatogonia. During the prospermatogonia to spermatogonia transition, prospermatogonia give rise to differentiating or undifferentiated spermatogonia. Thus, we examined whether *1a*Δ/Δ; *1b*Δ/Δ male germ cells can differentiate into spermatogonia. Seminiferous tubules of P7 testes were stained with an antibody against PLZF (Buaas et al., 2004; Costoya et al., 2004), a marker for undifferentiated spermatogonia, and with an antibody against c-KIT, a marker of differentiating spermatogonia (Schrans-Stassen et al., 1999), in combination with a TRA98 antibody (Figure 4J). TRA98+ cells were present in control and mutant tubules at P7. PLZF+ and c-KIT+ cells were abundant in control tubules but were not detected in mutant tubules (Figure 4J). To quantitatively evaluate PLZF+ and c-KIT+ cell populations, we performed fluorescence-activated cell sorting (Figures 4K and 4L). TRA98+ germ cells were sorted from P7 testicular cells (Figure 4K), and were then analyzed using antibodies against PLZF and c-KIT (Figure 4L). JMJD1A/JMJD1B depletion reduced germ cell numbers to about half that in control testes (Figure 4K), consistent with Figures 4C and 4E. Population analysis indicated that the c-KIT+/PLZF− cell population, representing differentiating spermatogonia, was predominant in P7 control germ cells, constituting approximately 40% of all cells (Figure 4L, top). The c-KIT-/PLZF+ population, representing undifferentiated spermatogonia, constituted approximately 20% of all cells in the control testes (Figure 4L, top). In addition, we found another population (~30%) composed of c-KIT+/PLZF+ cells. This population might represent an intermediate type of cell between undifferentiated spermatogonia and differentiating spermatogonia (Figure 4L, top). Strikingly, c-KIT+/PLZF−, c-KIT-/PLZF+, and c-KIT+/PLZF+ populations were almost absent in *1a*Δ/Δ; *1b*Δ/Δ germ cells at P7 (Figure 4L, bottom). Instead, the c-KIT−/PLZF− population was predominant in *1a*Δ/Δ; *1b*Δ/Δ germ cells, constituting approximately 80% of all cells. This c-KIT−/PLZF− population was barely detected in control testes (Figure 4L, top).

To determine the cellular characteristics of JMJD1A/JMJD1B-depleted germ cells, we performed mRNA sequencing (mRNA-seq) analysis using germ cells purified

incorporating EdU were counterstained with a TRA98 antibody and DAPI. Scale bars, 50 μm. (I) Average numbers of EdU+ cells per cross-tubular section are summarized. Error bars represent ± SEM (n = 3 mice each). ***p < 0.001 (t test).

(J) Whole-mount immunofluorescence analysis of seminiferous tubules from P7 control (*1a*Δ/+; *1b*Δ/+, top) and P7 mutant (*1a*Δ/Δ; *1b*Δ/Δ, bottom) testes. A TRA98 antibody was used to mark germ cells. Antibodies against PLZF and c-KIT were used to detect undifferentiated spermatogonia and differentiating spermatogonia, respectively. Nuclei were counterstained with DAPI.

(K and L) Population analysis of P7 germ cells by fluorescence-activated cell sorting (FACS). Germ cells were dissociated from control (top) and mutant testes (bottom), stained with a TRA98 antibody and antibodies against PLZF and c-KIT, and then used for FACS analysis. (K) P7 testicular cells were fractionated to examine cell profiles for forward scatter (FSC) and TRA98 staining. Boxes represent the germ cell population. (L) Population analysis of P7 male germ cells. TRA98-sorted germ cells (boxes shown in K) were used for the classification of PLZF+ undifferentiated spermatogonia and c-KIT+ differentiating spermatogonia.

(M) PCA plot visualizing the degree of dissimilarity of gene expression in male germ cells between the indicated genotypes and developmental times.

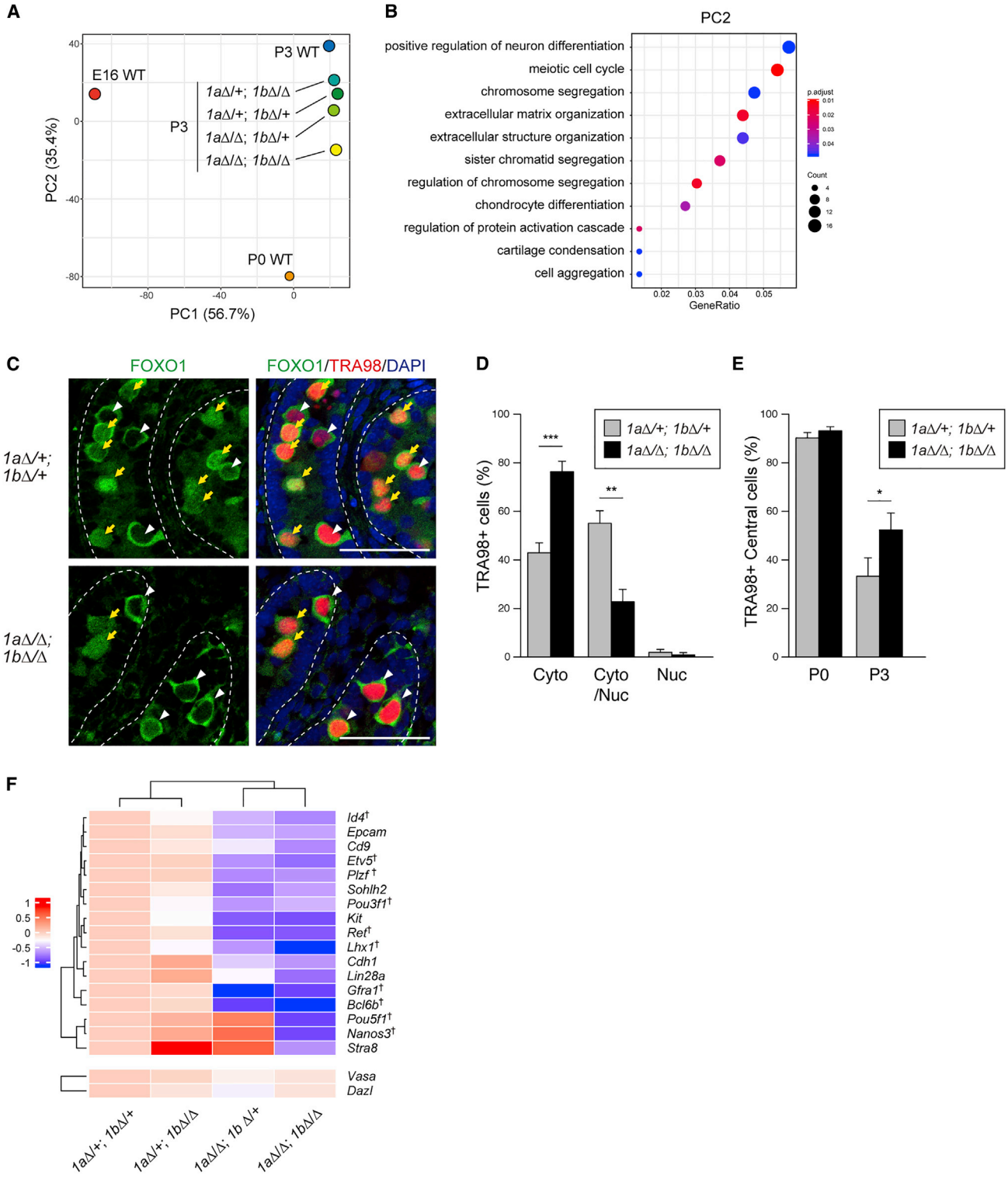

Figure 5. JMJD1A/JMJD1B Depletion Perturbs the Prospermatogonia to Spermatogonia Transition

(A) A PCA plot was used to visualize the degree of gene expression dissimilarity in male germ cells between the indicated genotypes and developmental times. We extracted differentially expressed genes between P0 WT and P3 WT and used them for PCA.

(legend continued on next page)

from P7 testes. We compared the gene expression of *1a*Δ/Δ; *1b*Δ/Δ germ cells with that of wild-type germ cells at several developmental stages by principal-component analysis (PCA). For this analysis, we utilized previously published mRNA-seq data of wild-type neonatal prospermatogonia (P0 WT), P7 wild-type c-KIT− spermatogonia (P7 WT [c-KIT−]), and P7 wild-type c-KIT+ spermatogonia (P7 WT [c-KIT+]) (Kubo et al., 2015). In addition to these data, we prepared mRNA-seq data of wild-type germ cells purified from P3 testis of this study (P3 WT) (Figure 4M). Genes that respond to environmental and biological stimuli were significantly enriched both in PC1 and PC2 (Figure S4). We noticed similar distances between P0 WT, P3 WT, and P7 WT. Interestingly, the distance from P7 *1a*Δ/Δ; *1b*Δ/Δ to P3 WT was much closer than that from P7 *1a*Δ/Δ; *1b*Δ/Δ to P7 WT (c-KIT+ or c-KIT−) (Figure 4M), indicating that the prospermatogonia to spermatogonia transition was perturbed by JMJD1A/JMJD1B depletion. Considering that *1a*Δ/Δ; *1b*Δ/Δ germ cells did not enter the first round of spermatogenesis (Figure 4D) and did not express typical spermatogonia markers (Figure 4L), JMJD1A/JMJD1B depletion might inhibit the generation of functional spermatogonia.

JMJD1A/JMJD1B Depletion Perturbs the Prospermatogonia to Spermatogonia Transition

To address how JMJD1 isozymes control the prospermatogonia to spermatogonia transition, we performed transcriptomic analysis of postnatal germ cells lacking JMJD1A and/or JMJD1B. In brief, *1a*Δ/+; *1b*Δ/+, *1a*Δ/+; *1b*Δ/Δ, *1a*Δ/Δ; *1b*Δ/+, and *1a*Δ/Δ; *1b*Δ/Δ germ cells were isolated from the corresponding P3 testes by immunoaffinity purification, and were then subjected to mRNA-seq analysis. For PCA, we used previously published datasets for E16 prospermatogonia (E16 WT) and P0 WT (Kubo et al., 2015), and a P3 WT dataset prepared in this study. We extracted differentially expressed genes between P0 WT and P3 WT, and then merged our transcriptome datasets for P3 germ cells (Figure 5A). As shown in Figure 5A, serial mutants of P3 germ cells were located near the line connecting P0 to P3. Of these, *1a*Δ/Δ; *1b*Δ/+ was further away from P3 WT than *1a*Δ/+; *1b*Δ/Δ, indicating that JMJD1A is more crucial than JMJD1B in this process. Importantly, among the mutants, *1a*Δ/Δ; *1b*Δ/Δ was farthest from P3 WT and nearest to P0 WT (Figure 5A), indicating that the loss of all four *Jmjd1* alleles induced the most severe developmental delay from P0 to P3. Notably, the PCA plot showed that PC2 (y axis) mainly contributed to the P0 to P3 transition (Figure 5A). Genes related to neuron differentiation, meiosis, and chromosome segregation were significantly enriched in PC2 (Figure 5B); therefore, perturbed expression of these genes might account for the developmental delay of germ cells lacking JMJD1A and/or JMJD1B.

To further confirm the requirement of JMJD1 isozymes for prospermatogonia to spermatogonia transition, we examined the subcellular localization of FOXO1, a marker of prospermatogonia/spermatogonia (Figures 5C and 5D). FOXO1 translocates from the cytoplasm to the nucleus during the prospermatogonia to c-KIT− spermatogonia transition (Goertz et al., 2011). In control P3 germ cells, a population in which FOXO1 was present in the cytoplasm and nucleus reached over 50%. In contrast, in *1a*Δ/Δ; *1b*Δ/Δ germ cells, this population was minor (∼20%) but another population in which FOXO1 was detected only in the cytoplasm was predominant (∼80%) (Figure 5D). This cytological analysis confirmed perturbation of the prospermatogonia to spermatogonia transition in *1a*Δ/Δ; *1b*Δ/Δ germ cells. Prospermatogonia migrate into the basement membrane to form an SSC pool in seminiferous tubules during the prospermatogonia to spermatogonia transition. To address whether this process was inhibited by JMJD1A/JMJD1B depletion, we examined the intratubular localization of germ cells in P0 and P3 testes. No significant difference in intratubular localization was observed

(B) Gene ontology analysis of genes contributing to PC2 shown in Figure 5A. We calculated the loading of PC2 and used the top 5% of genes for gene ontology analysis.

(C) Immunofluorescence analysis of FOXO1 subcellular localization in control and JMJD1A/JMJD1B-depleted germ cells at P3. We classified localization patterns of FOXO1 as cytoplasmic (indicated by white arrowheads), nuclear, or both (indicated by yellow arrows). Scale bars, 50 μm.

(D) Comparative evaluation of the subcellular localization of FOXO1 between control and JMJD1A/JMJD1B-depleted germ cells. Error bars represent ± SEM (n = 3 mice per genotype).

(E) Intratubular localization of prenatal and postnatal germ cells in the seminiferous tubule. Control and mutant testes sections at the indicated developmental times were stained with antibodies to TRA98 and DAPI. "Peri" and "Central" represent TRA98+ germ cells in contact with the basement membrane and not in contact with the basement membrane, respectively. Error bars represent ± SEM (n = 3 mice per indicated genotype and developmental time).

(F) Expression of spermatogonial stem cell marker genes in postnatal male germ cells was visualized with a heatmap. mRNA-seq data of P3 germ cells of the indicated genotypes was utilized. *Vasa* and *Dazl* were used as pan-germ cell marker genes. Daggers represent genes required for the maintenance of male germ cells. The heatmap represents log2-transformed FPKM values of each sample normalized to those of the control.

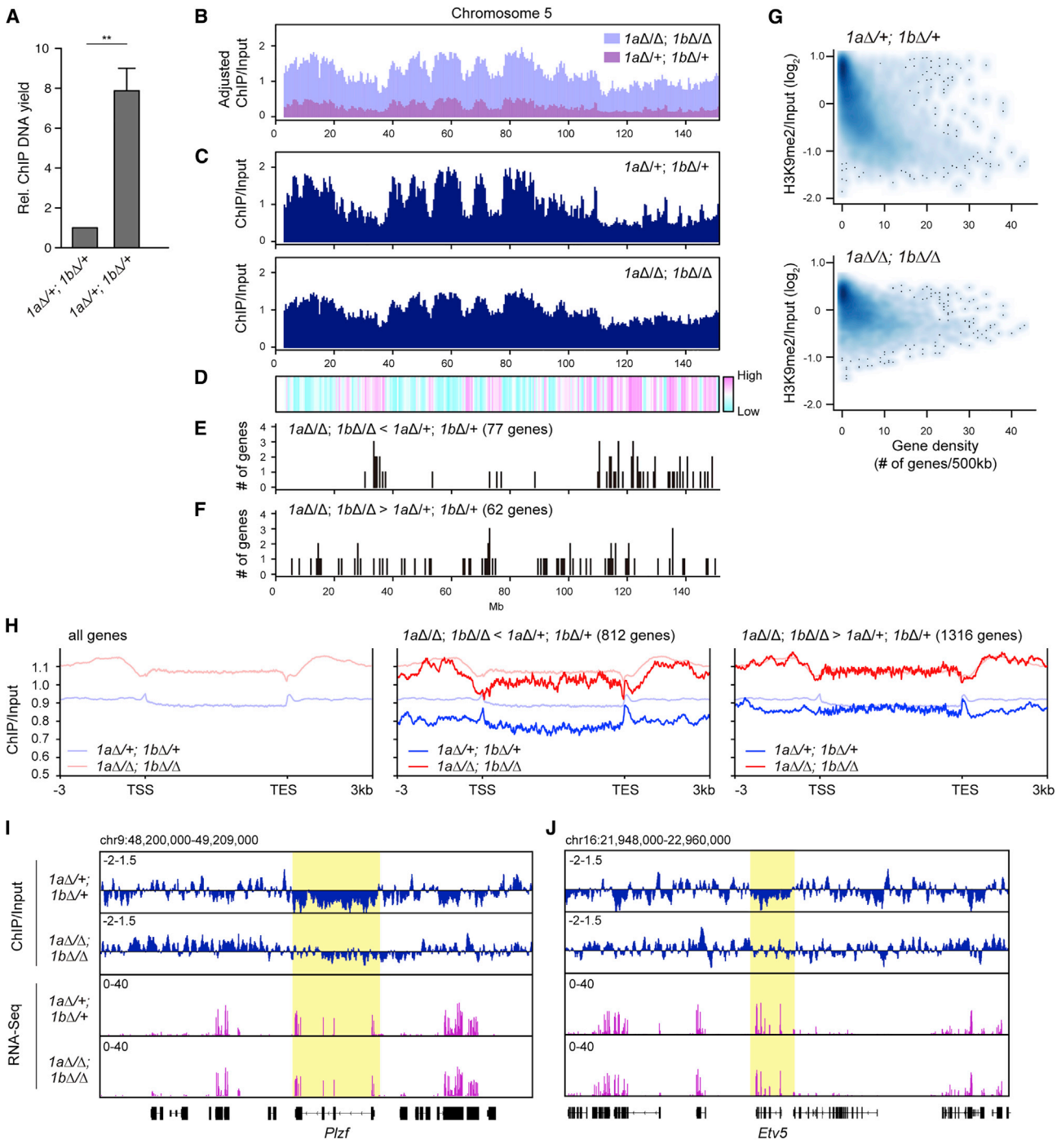

Figure 6. JMJD1 Isozymes Preferentially Activate Transcription in Gene-Dense Chromosomal Regions in Prospermatogonia

(A) P3 germ cells of the indicated genotypes were subjected to native ChIP analysis with an anti-H3K9me2 antibody and the yield of ChIP DNA was quantified. DNA collected from control cells was assumed as 1 for data normalization. Data are presented as the mean ± SEM (n = 3 independent experiments.) **p < 0.01 (t test).

(B–F) Correlation between H3K9me2 distribution and JMJD1A/JMJD1B-regulated genes in prospermatogonia. P3 germ cells were isolated from control (1aΔ/+; 1bΔ/+) and JMJD1A/JMJD1B-depleted (*1a*Δ/Δ; *1b*Δ/Δ) germ cells at P3 for ChIP-seq analysis of H3K9me2. We used a genomic view of chromosome 5 as representative data. Data were normalized (B) and not normalized (C) according to the amount of immunoprecipitated DNA. (D) Heatmap showing the log2-transformed ratio of ChIP/input of JMJD1A/JMJD1B-depleted germ cells divided

(legend continued on next page)

between mutant and control germ cells at P0 (Figure 5E). In contrast, ~70% of control germ cells had migrated into the basement membrane, whereas only ~50% of mutant cells had migrated at P3, further confirming that the prospermatogonia to spermatogonia transition was perturbed by JMJD1A/JMJD1B depletion.

To understand how JMJD1A/JMJD1B depletion affects the expression of SSC marker genes, we compared mRNA levels of P3 germ cells by heatmap analysis (Figure 5F). The expression levels of pan-germ cell marker genes, such as *Vasa* and *Dazl*, were not affected by JMJD1A/JMJD1B depletion, whereas the expression levels of SSC marker genes were significantly reduced in *1a*Δ/Δ; *1b*Δ/Δ cells (Figure 5F), indicating that JMJD1A/JMJD1B selectively and positively regulates SSC marker genes during the prospermatogonia to spermatogonia transition. Notably, reduced expression of SSC maker genes was more prominent in *1a*Δ/Δ; *1b*Δ/+ cells than in *1a*Δ/+; *1b*Δ/Δ cells, indicating a predominant role of JMJD1A in the activation of SSC marker genes. Among these genes, several are required for SSC maintenance (as discussed later). We speculate that the inactivation of multiple SSC maintenance genes may account for the failure of functional spermatogonia development in *1a*Δ/Δ; *1b*Δ/Δ germ cells.

To investigate the cause of the disturbed prospermatogonia to spermatogonia transition, we performed proliferation and cell death analyses in mutant testes at P3 (Figures S5A and S5B). EdU incorporation analysis indicated decreased proliferation of *1a*Δ/Δ; *1b*Δ/Δ germ cells in P3 testes (Figures S5A). In contrast, the frequency of apoptotic cells was not changed by JMJD1A/JMJD1B depletion (Figure S5B). These data indicate that perturbed prospermatogonia to spermatogonia transition in *1a*Δ/Δ; *1b*Δ/Δ germ cells might occur by inhibition of cell-cycle progression. A mitotic wave is initiated in male germ cells after birth; therefore, dysregulation of the genes related to chromosomal segregation (Figure 5B) might inhibit this mitotic wave in *1a*Δ/Δ; *1b*Δ/Δ germ cells.

JMJD1 Isozymes Preferentially Activate Transcription in Gene-Dense Regions of Chromosomes in Prospermatogonia

To examine the contribution of JMJD1-mediated H3K9me2 demethylation to transcription at the single-gene level, we performed H3K9me2 chromatin immunoprecipitation sequencing (ChIP-seq) analysis using purified P3 male germ cells. H3K9me2 ChIP analysis demonstrated that an 8- to 10-fold greater amount of DNA was immunoprecipitated from *1a*Δ/Δ; *1b*Δ/Δ cells compared with control cells (Figure 6A). This is in accord with the immunofluorescence analysis of H3K9me2 (Figure 2D). We present two patterns of H3K9me2 distribution. First is the absolute distribution of H3K9me2, in which data were normalized to the immunoprecipitated amounts of DNA (Figure 6B, chromosome 5 was used as a representative chromosome). Second is the relative distribution of H3K9me2, in which similar numbers of reads from control and mutant cells are displayed (approximately 40 million reads) (Figure 6C). As shown in Figure 6B, an increase in H3K9me2 was prominent throughout chromosome 5, indicating that JMJD1 isozymes target global regions of chromosomes. Relative H3K9me2 distribution profiles showed that H3K9me2 was unevenly distributed in P3 control germ cells, with H3K9me2-high and -low regions (Figure 6C). Next, we calculated the fold increase of H3K9me2 induced by JMJD1A/JMJD1B depletion by dividing the H3K9me2 value of *1a*Δ/Δ; *1b*Δ/Δ cells by that of control cells (Figure 6D). We found that chromosomal regions preferentially demethylated by JMJD1A/JMJD1B (shown in red in Figure 6D) overlap with originally H3K9me2-low regions in control cells (Figure 6C).

Gene expression analysis demonstrated that 812 and 1,316 genes were down- and upregulated in *1a*Δ/Δ; *1b*Δ/Δ P3 germ cells compared with *1a*Δ/+; *1b*Δ/+ P3 germ cells, respectively (listed in Table S1). The former and latter genes are hereafter referred to as dKO < Ctrl and dKO > Ctrl, respectively. Mapping analysis of JMJD1A/JMJD1B-regulated genes on chromosome 5 revealed that dKO < Ctrl genes were enriched in the regions where H3K9me2 was preferentially demethylated by JMJD1A/JMJD1B (Figures 6D and 6E), but this feature was not found in dKO > Ctrl genes (Figures 6D and 6F).

We previously demonstrated that JMJD1 isozymes preferentially targeted gene-dense regions of chromosomes in embryonic stem cells (Kuroki et al., 2018). To determine whether this feature was conserved in prospermatogonia, we examined the correlation between gene density and

by that of control germ cells. (E and F) Chromosomal distribution of genes that were downregulated (E) and upregulated (F) in *1a*Δ/Δ; *1b*Δ/Δ P3 germ cells compared with those in *1a*Δ/+; *1b*Δ/+ P3 germ cells.

(G) Correlation between gene density and H3K9me2 levels in control germ cells (top) and JMJD1A/JMJD1B-depleted germ cells (bottom). The x and y axes indicate the number of mm10 RefSeq genes and the ChIP/input ratio of H3K9me2, respectively.

(H) Averaged profile of H3K9me2 around the gene bodies of control (*1a*Δ/+; *1b*Δ/+: blue) and JMJD1A/JMJD1B-depleted (*1a*Δ/Δ; *1b*Δ/Δ: red) germ cells. H3K9me2 profiles of all genes (left), downregulated (middle) and upregulated (right) in *1a*Δ/Δ; *1b*Δ/Δ P3 germ cells compared with that in *1a*Δ/+; *1b*Δ/+ P3 germ cells are presented.

(I and J) Distribution profile of H3K9me2 and expression profile for the *Plzf* (I) and *Etv5* (J) loci. Log2-transformed ratios of ChIP/Input (top) and FPKM counts from RNA-seq analysis (bottom) are shown.

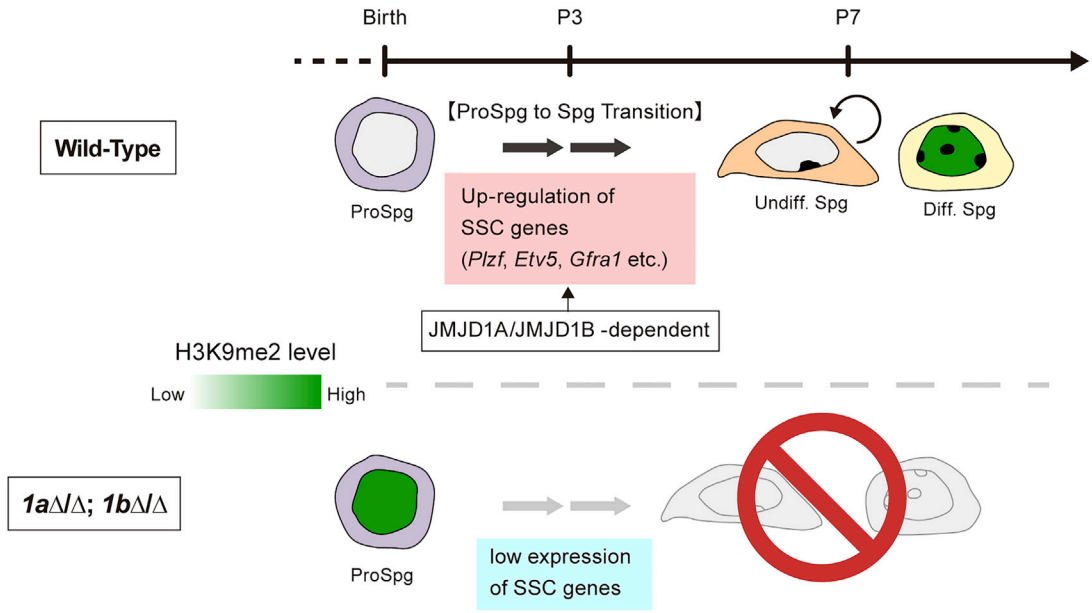

Figure 7. Role of JMJD1A and JMJD1B in the Prospermatogonia to Spermatogonia Transition

In wild-type spermatogonia, JMJD1A and JMJD1B are highly expressed and the H3K9me2 mark is removed to extremely low levels in a JMJD1-dependent manner. This H3K9 hypomethylation status is critical for upregulation of SSC genes and the subsequent transition of prospermatogonia to spermatogonia after birth. In JMJD1A/JMJD1B-depleted spermatogonia, H3K9me2 is hypermethylated, resulting in low SSC gene expression and perturbed differentiation of prospermatogonia.

H3K9me2 in P3 germ cells (Figure 6G). There was an inverse relationship between gene density and H3K9me2 levels in control germ cells (Figure 6G, top). Importantly, this feature was dampened by JMJD1A/JMJD1B depletion (Figure 6G, bottom), indicating that JMJD1 isozymes preferentially target gene-dense regions of chromosomes in prospermatogonia.

We next examined the correlation between altered gene expression and altered H3K9me2 levels in JMJD1A/JMJD1B-depleted male germ cells at P3 (Figure 6H). As H3K9me2 levels in dKO > Ctrl genes were similar to those in all genes, upregulation of dKO > Ctrl genes might occur independently of H3K9 demethylation. In contrast, H3K9me2 levels were markedly lower in dKO < Ctrl genes compared with all genes, indicating that H3K9me2 in dKO < Ctrl genes was more actively targeted by JMJD1 isozymes compared with H3K9me2 in other loci. Finally, we examined the impact of JMJD1A/JMJD1B-mediated H3K9 demethylation on gene expression at the single-gene level. For this purpose, genomic loci around *Plzf* and *Etv5* were chosen as representative regions (Figures 6I and 6J, respectively) because the expression levels of these SSC marker genes were downregulated by JMJD1A/JMJD1B depletion (Figure 5H). In control cells, H3K9me2 levels of *Plzf* and *Etv5* gene bodies were much lower than those of adjacent genes. In *1a*Δ/Δ; *1b*Δ/Δ cells, the increase of H3K9me2 was more remarkable in *Plzf* and *Etv5* gene bodies compared with adjacent genes (Figures 6I and 6J). Importantly, the expression levels of *Plzf* and *Etv5* were reduced but those of adjacent genes were not affected by JMJD1A/JMJD1B depletion. As shown in Figure S6, these characteristics were also found in SSC marker genes whose expression was regulated by JMJD1A/JMJD1B. Collectively, the transcriptional activation of SSC marker genes in prospermatogonia is highly dependent on JMJD1A/JMJD1B-mediated H3K9 demethylation.

DISCUSSION

Our present studies are summarized in Figure 7. We propose that activation of SSC maintenance genes in prospermatogonia is critical for the subsequent differentiation into spermatogonia. JMJD1A and JMJD1B are redundant but substantially contribute to activation of these genes by removing repressive H3K9 methylation marks. Depletion of JMJD1A/JMJD1B results in increased H3K9 methylation and decreased transcription of SSC maintenance genes, thereby blocking the generation of functional (i.e., undifferentiated and differentiating) spermatogonia. Below, we discuss our results with reference to recent findings related to epigenetic regulation and germ cell development.

We previously demonstrated that the GLP/G9a complex is responsible for global H3K9me2 in embryonic stem cells

(Tachibana et al., 2002, 2005). Recently, we reported that JMJD1A/JMJD1B contributed to transcriptional activation by demethylating H3K9me2 marks deposited by GLP/G9a (Kuroki et al., 2018). We speculate that JMJD1A/JMJD1B-mediated H3K9 demethylation may also counteract GLP/G9a complex-mediated H3K9 methylation in spermatogonia development. In support of this, the GLP/G9a complex is expressed in postnatal spermatogonia (Tachibana et al., 2007). Alternatively, Suv39h1 and Eset H3K9 methyltransferases are candidate enzymes that might counteract JMJD1A/JMJD1B-mediated H3K9 demethylation in prospermatogonia because Suv39h1 (Peters et al., 2001) and Eset (Liu et al., 2014) are expressed in premeiotic spermatogonia. To comprehensively examine the role of H3K9 methylation dynamics in spermatogonia development, it is important to identify which H3K9 methyltransferase counteracts JMJD1-mediated H3K9 demethylation.

In this study, we demonstrated partial non-redundancy of JMJD1 isozymes in spermatogenesis. As shown in Figure 3H, *1a*Δ/+; *1b*Δ/Δ germ cells could differentiate into mature sperm and the corresponding male mice were fertile. In contrast, *1a*Δ/Δ; *1b*Δ/+ germ cells could not complete meiosis and the corresponding male mice were infertile. These data indicate a predominant function of JMJD1A in postnatal spermatogenesis. Loss of all four *Jmjd1a* and *Jmjd1b* alleles resulted in the most severe postnatal male germ cell developmental phenotype, i.e., exhaustion of germ cells before puberty, indicating the redundancy of JMJD1A and JMJD1B in the maintenance of male germ cells. This phenotype was associated with a marked inhibition of first-round spermatogenesis (Figure 4D) and a lack of functional spermatogonia (Figure 4L). Many studies have demonstrated that spermatogonia express specific marker genes related to transcription factors and cell surface receptors. Of these, several transcription factors, including *Oct4* (Dann et al., 2008), *Id4* (Oatley et al., 2011), *Ret* (Jain et al., 2004), *Gfra1* (Naughton et al., 2006), *Plzf* (Buaas et al., 2004; Costoya et al., 2004), *Etv5* (Morrow et al., 2007), *Lhx1* (Oatley et al., 2007), and *Bcl6b* (Oatley et al., 2006), have important roles in maintaining the male germline. Interestingly, expression levels of these genes were significantly reduced in *1a*Δ/Δ; *1b*Δ/Δ germ cells (Figure 5F). The decreased expression of multiple spermatogonia-specific transcription factors might synergistically affect the cellular integrity of the male germline in JMJD1A/JMJD1B-depleted germ cells.

DNA methylation levels change dynamically throughout the reproductive cycle (Seisenberger et al., 2013). Several studies, including ours, also reveal that H3K9me2 levels are dynamically regulated during the reproductive cycle. First, we demonstrated that JMJD1A and JMJD1B redundantly control embryogenesis around the peri-implantation period, where JMJD1 isozymes have crucial roles during epiblast development (Kuroki et al., 2018). Second, JMJD1A contributes to sex determination by activating *Sry* in gonadal somatic cells at E11.5. JMJD1A deficiency resulted in the failure of H3K9 demethylation at the *Sry* locus and the failure of *Sry* activation, thereby inducing male-to-female sex reversal (Kuroki et al., 2013). Third, JMJD1A contributed to the elongation step of spermatogenesis by activating genes required for the histone to protamine transition (Liu et al., 2010; Okada et al., 2007). Finally, we show that JMJD1 isozymes substantially contribute to the prospermatogonia to spermatogonia transition. In summary, the dynamic regulation of H3K9me2 plays a critical role in various steps of the reproductive cycle. In addition to H3K9 methylation enzymes, there are many other types of histone K methylating and counteracting demethylating enzymes in mammals (Dillon et al., 2005; Kooistra and Helin, 2012). Therefore, it is likely that histone K methylation marks other than H3K9 methylation are also dynamically regulated during development and cell differentiation. The next important step is, therefore, to identify these methylating/demethylating enzymes and their target loci.

EXPERIMENTAL PROCEDURES

Antibodies

The following antibodies were used were used for immunoblotting. Anti-SOX9 (Merck Millipore, AB5535), anti-HSD3b (TransGenic, KO607), anti-TRA98 (Abcam, ab82527), anti-FLAG (clone M2, Sigma, A8592), anti-VASA (Abcam, ab13840), anti-EPCAM (clone G8.8, eBioscience, no. 14-5791-85), anti-FOXO1 (CST, no. 2880), anti-PLZF (Santa Cruz, H300), anti-c-KIT (BioLegend, no. 105803), anti-JMJD1B (Abvnova, PAB15833), anti-H3K9me1 (Abcam, ab9045), anti-H3K9me2 (clone 6D11) (Kimura et al., 2008), anti-H3K9me3 (clone 2F3) (Kimura et al., 2008), anti-JMJD1A (clone F0618) (Abe et al., 2015), and anti-JMJD1B (Abvnova, PAB15833). Anti-H3K9me2 (Abcam, Ab1220) was used for ChIP analysis.

Mice

For the generation of *Jmjd1a*^{2lox} and *Jmdj1b*^{2lox} mice, *Jmjd1a* and *Jmjd1b* knockin targeting vectors were constructed using bacterial artificial chromosome recombineering (Copeland et al., 2001). Vectors were introduced into TT2 embryonic stem cells. Chimeric males derived from homologously recombined embryonic stem cell clones were obtained to generate F1 offspring bearing the mutant alleles, which were further backcrossed to C57BL/6 for more than five generations. *Jmjd1b*$^{FLAG-KI}$ (Kuroki et al., 2018), *Vasa-Cre* Tg (Gallardo et al., 2007), and *Oct4-EGFP* Tg mice (Yoshimizu et al., 1999) were described previously. All animal experiments were performed under the animal ethical guidelines of Osaka University, Tokushima University and Kyoto University.

Data and Code Availability

The RNA-seq and ChIP-seq data are deposited in the Gene Expression Omnibus database under accession number GSE148055.

SUPPLEMENTAL INFORMATION

Supplemental Information can be found online at https://doi.org/10.1016/j.stemcr.2020.06.013.

AUTHOR CONTRIBUTIONS

S. Kuroki and M.T. designed the experiments. S. Kuroki, Y.M., S. Kitano, H.M., and M.T. performed the experiments. S. Kuroki and R.M. analyzed the data. M.F. and Y.S. provided resources. S. Kuroki and M.T. wrote the manuscript. M.T. supervised the project and approved the manuscript.

ACKNOWLEDGMENTS

We thank all members of the Tachibana laboratory. This work was supported by JSPS KAKENHI grant numbers JP26250037 (M.T.), JP16H01218 (M.T.), JP16H01409 (M.T.), JP17H06424 (M.T.), JP16K21196 (S. Kuroki), JP20H05364 (S. Kuroki) and JP20H03262 (S. Kuroki); the Funding Program for Next Generation World-Leading Researchers (M.T.); the Takeda Science Foundation (M.T. and S. Kuroki); the Suntory Foundation for life sciences (S. Kuroki); and a Promotion of Science Cooperative Research Grant of the Institute for Enzyme Research, Joint Usage/Research Center, Tokushima University (H.M.). We thank Edanz Group (https://en-author-services.edanzgroup.com/) for editing a draft of this manuscript.

Received: September 19, 2019
Revised: June 15, 2020
Accepted: June 15, 2020
Published: July 16, 2020

REFERENCES

Abe, Y., Rozqie, R., Matsumura, Y., Kawamura, T., Nakaki, R., Tsurutani, Y., Tanimura-Inagaki, K., Shiono, A., Magoori, K., Nakamura, K., et al. (2015). JMJD1A is a signal-sensing scaffold that regulates acute chromatin dynamics via SWI/SNF association for thermogenesis. Nat. Commun. *6*, 7052.

Buaas, F.W., Kirsh, A.L., Sharma, M., McLean, D.J., Morris, J.L., Griswold, M.D., de Rooij, D.G., and Braun, R.E. (2004). Plzf is required in adult male germ cells for stem cell self-renewal. Nat. Genet. *36*, 647–652.

Copeland, N.G., Jenkins, N.A., and Court, D.L. (2001). Recombineering: a powerful new tool for mouse functional genomics. Nat. Rev. Genet. *2*, 769–779.

Costoya, J.A., Hobbs, R.M., Barna, M., Cattoretti, G., Manova, K., Sukhwani, M., Orwig, K.E., Wolgemuth, D.J., and Pandolfi, P.P. (2004). Essential role of Plzf in maintenance of spermatogonial stem cells. Nat. Genet. *36*, 653–659.

Dann, C.T., Alvarado, A.L., Molyneux, L.A., Denard, B.S., Garbers, D.L., and Porteus, M.H. (2008). Spermatogonial stem cell self-renewal requires OCT4, a factor downregulated during retinoic acid-induced differentiation. Stem Cells *26*, 2928–2937.

de Rooij, D.G. (1998). Stem cells in the testis. Int. J. Exp. Pathol. *79*, 67–80.

Deguchi, K., Nagamatsu, G., Miyachi, H., Kato, Y., Morita, S., Kimura, H., Kitano, S., Hatada, I., Saga, Y., Tachibana, M., et al. (2013). Posttranscriptional regulation of histone lysine methyltransferase GLP in embryonic male mouse germ cells. Biol. Reprod. *88*, 36.

Dillon, S.C., Zhang, X., Trievel, R.C., and Cheng, X. (2005). The SET-domain protein superfamily: protein lysine methyltransferases. Genome Biol. *6*, 227.

Gallardo, T., Shirley, L., John, G.B., and Castrillon, D.H. (2007). Generation of a germ cell-specific mouse transgenic Cre line, Vasa-Cre. Genesis *45*, 413–417.

Goertz, M.J., Wu, Z., Gallardo, T.D., Hamra, F.K., and Castrillon, D.H. (2011). Foxo1 is required in mouse spermatogonial stem cells for their maintenance and the initiation of spermatogenesis. J. Clin. Invest. *121*, 3456–3466.

Jain, S., Naughton, C.K., Yang, M., Strickland, A., Vij, K., Encinas, M., Golden, J., Gupta, A., Heuckeroth, R., Johnson, E.M., Jr., et al. (2004). Mice expressing a dominant-negative Ret mutation phenocopy human Hirschsprung disease and delineate a direct role of Ret in spermatogenesis. Development *131*, 5503–5513.

Kimura, H., Hayashi-Takanaka, Y., Goto, Y., Takizawa, N., and Nozaki, N. (2008). The organization of histone H3 modifications as revealed by a panel of specific monoclonal antibodies. Cell Struct. Funct. *33*, 61–73.

Kooistra, S.M., and Helin, K. (2012). Molecular mechanisms and potential functions of histone demethylases. Nat. Rev. Mol. Cell Biol. *13*, 297–311.

Kubo, N., Toh, H., Shirane, K., Shirakawa, T., Kobayashi, H., Sato, T., Sone, H., Sato, Y., Tomizawa, S., Tsurusaki, Y., et al. (2015). DNA methylation and gene expression dynamics during spermatogonial stem cell differentiation in the early postnatal mouse testis. BMC Genomics *16*, 624.

Kuroki, S., Matoba, S., Akiyoshi, M., Matsumura, Y., Miyachi, H., Mise, N., Abe, K., Ogura, A., Wilhelm, D., Koopman, P., et al. (2013). Epigenetic regulation of mouse sex determination by the histone demethylase Jmjd1a. Science *341*, 1106–1109.

Kuroki, S., Nakai, Y., Maeda, R., Okashita, N., Akiyoshi, M., Yamaguchi, Y., Kitano, S., Miyachi, H., Nakato, R., Ichiyanagi, K., et al. (2018). Combined loss of JMJD1A and JMJD1B reveals critical roles for H3K9 demethylation in the maintenance of embryonic stem cells and early embryogenesis. Stem Cell Reports *10*, 1340–1354.

Liu, Z., Zhou, S., Liao, L., Chen, X., Meistrich, M., and Xu, J. (2010). Jmjd1a demethylase-regulated histone modification is essential for cAMP-response element modulator-regulated gene expression and spermatogenesis. J. Biol. Chem. *285*, 2758–2770.

Liu, S., Brind'Amour, J., Karimi, M.M., Shirane, K., Bogutz, A., Lefebvre, L., Sasaki, H., Shinkai, Y., and Lorincz, M.C. (2014). Setdb1 is required for germline development and silencing of H3K9me3-marked endogenous retroviruses in primordial germ cells. Genes Dev. *28*, 2041–2055.

Morrow, C.M., Hostetler, C.E., Griswold, M.D., Hofmann, M.C., Murphy, K.M., Cooke, P.S., and Hess, R.A. (2007). ETV5 is required for continuous spermatogenesis in adult mice and may mediate blood testes barrier function and testicular immune privilege. Ann. N. Y. Acad. Sci. *1120*, 144–151.

Naughton, C.K., Jain, S., Strickland, A.M., Gupta, A., and Milbrandt, J. (2006). Glial cell-line derived neurotrophic factor-

mediated RET signaling regulates spermatogonial stem cell fate. Biol. Reprod. *74*, 314–321.

Oatley, J.M., Avarbock, M.R., Telaranta, A.I., Fearon, D.T., and Brinster, R.L. (2006). Identifying genes important for spermatogonial stem cell self-renewal and survival. Proc. Natl. Acad. Sci. U S A. *103*, 9524–9529.

Oatley, J.M., Avarbock, M.R., and Brinster, R.L. (2007). Glial cell line-derived neurotrophic factor regulation of genes essential for self-renewal of mouse spermatogonial stem cells is dependent on Src family kinase signaling. J. Biol. Chem. *282*, 25842–25851.

Oatley, M.J., Kaucher, A.V., Racicot, K.E., and Oatley, J.M. (2011). Inhibitor of DNA binding 4 is expressed selectively by single spermatogonia in the male germline and regulates the self-renewal of spermatogonial stem cells in mice. Biol. Reprod. *85*, 347–356.

Okada, Y., Scott, G., Ray, M.K., Mishina, Y., and Zhang, Y. (2007). Histone demethylase JHDM2A is critical for Tnp1 and Prm1 transcription and spermatogenesis. Nature *450*, 119–123.

Peters, A.H., O'Carroll, D., Scherthan, H., Mechtler, K., Sauer, S., Schofer, C., Weipoltshammer, K., Pagani, M., Lachner, M., Kohlmaier, A., et al. (2001). Loss of the Suv39h histone methyltransferases impairs mammalian heterochromatin and genome stability. Cell *107*, 323–337.

Schrans-Stassen, B.H., van de Kant, H.J., de Rooij, D.G., and van Pelt, A.M. (1999). Differential expression of c-kit in mouse undifferentiated and differentiating type A spermatogonia. Endocrinology *140*, 5894–5900.

Seisenberger, S., Peat, J.R., Hore, T.A., Santos, F., Dean, W., and Reik, W. (2013). Reprogramming DNA methylation in the mammalian life cycle: building and breaking epigenetic barriers. Philos. Trans. R. Soc. Lond. B Biol. Sci. *368*, 20110330.

Tachibana, M., Sugimoto, K., Nozaki, M., Ueda, J., Ohta, T., Ohki, M., Fukuda, M., Takeda, N., Niida, H., Kato, H., et al. (2002). G9a histone methyltransferase plays a dominant role in euchromatic histone H3 lysine 9 methylation and is essential for early embryogenesis. Genes Dev. *16*, 1779–1791.

Tachibana, M., Ueda, J., Fukuda, M., Takeda, N., Ohta, T., Iwanari, H., Sakihama, T., Kodama, T., Hamakubo, T., and Shinkai, Y. (2005). Histone methyltransferases G9a and GLP form heteromeric complexes and are both crucial for methylation of euchromatin at H3-K9. Genes Dev. *19*, 815–826.

Tachibana, M., Nozaki, M., Takeda, N., and Shinkai, Y. (2007). Functional dynamics of H3K9 methylation during meiotic prophase progression. EMBO J. *26*, 3346–3359.

Tanaka, H., Pereira, L.A., Nozaki, M., Tsuchida, J., Sawada, K., Mori, H., and Nishimune, Y. (1997). A germ cell-specific nuclear antigen recognized by a monoclonal antibody raised against mouse testicular germ cells. Int. J. Androl. *20*, 361–366.

Ueda, J., Tachibana, M., Ikura, T., and Shinkai, Y. (2006). Zinc finger protein Wiz links G9a/GLP histone methyltransferases to the corepressor molecule CtBP. J. Biol. Chem. *281*, 20120–20128.

Yamane, K., Toumazou, C., Tsukada, Y., Erdjument-Bromage, H., Tempst, P., Wong, J., and Zhang, Y. (2006). JHDM2A, a JmjC-containing H3K9 demethylase, facilitates transcription activation by androgen receptor. Cell *125*, 483–495.

Yoshida, S., Sukeno, M., Nakagawa, T., Ohbo, K., Nagamatsu, G., Suda, T., and Nabeshima, Y. (2006). The first round of mouse spermatogenesis is a distinctive program that lacks the self-renewing spermatogonia stage. Development *133*, 1495–1505.

Yoshimizu, T., Sugiyama, N., De Felice, M., Yeom, Y.I., Ohbo, K., Masuko, K., Obinata, M., Abe, K., Scholer, H.R., and Matsui, Y. (1999). Germline-specific expression of the Oct-4/green fluorescent protein (GFP) transgene in mice. Dev. Growth Differ. *41*, 675–684.

Stem Cell Reports, Volume *15*

Supplemental Information

H3K9 Demethylases JMJD1A and JMJD1B Control Prospermatogonia to Spermatogonia Transition in Mouse Germline

Shunsuke Kuroki, Ryo Maeda, Masashi Yano, Satsuki Kitano, Hitoshi Miyachi, Mikiko Fukuda, Yoichi Shinkai, and Makoto Tachibana

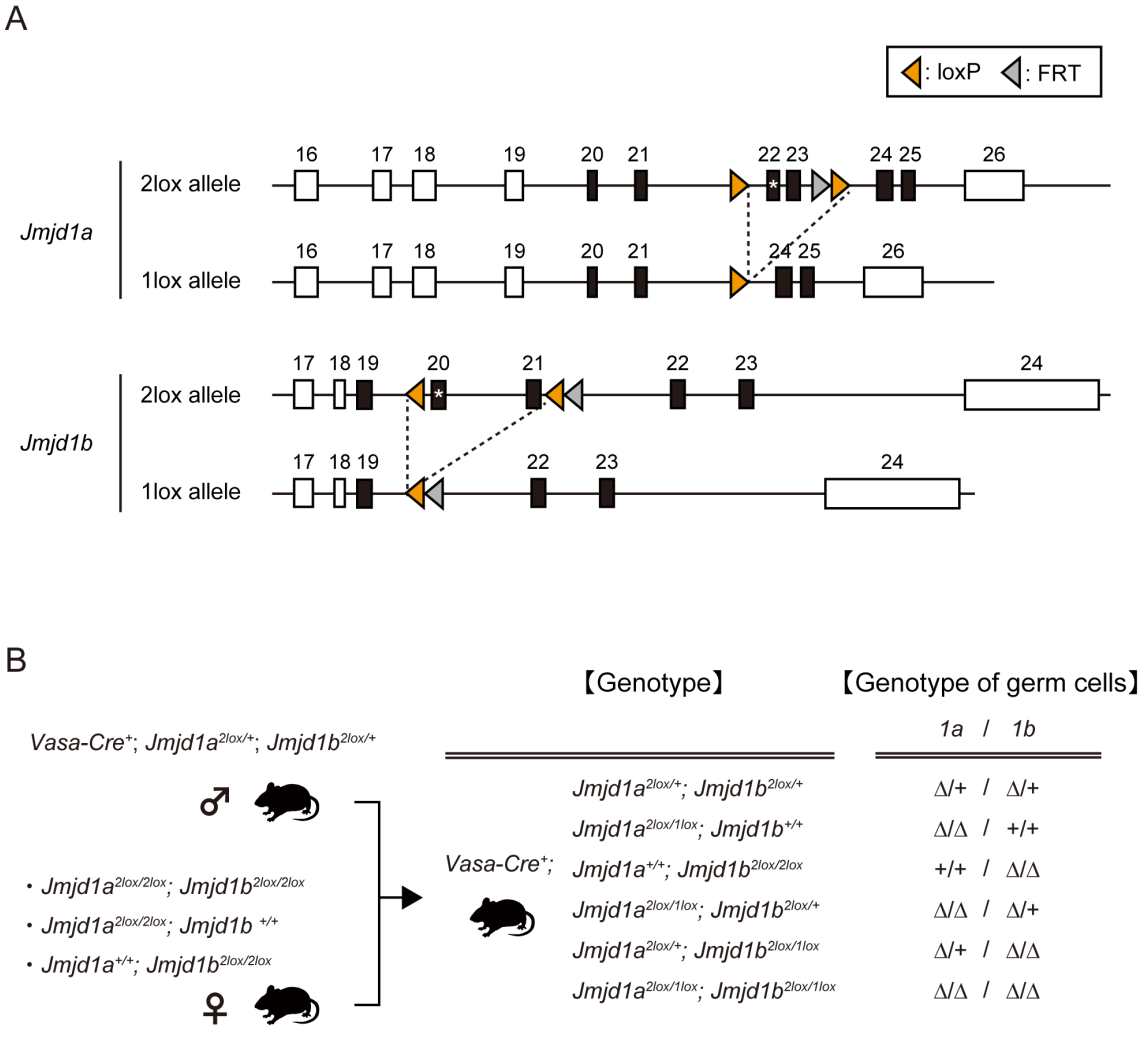

Supplementary Figure S1 (Related to Figure 2)

Generation of germline-specific knockout mice for *Jmjd1a* and *Jmjd1b*.

(A) 2lox conditional alleles and 1lox knockout alleles for *Jmjd1a* (top) and *Jmjd1b* (bottom). Black boxes represent exons corresponding to the JmjC domain. Asterisks represent exons corresponding to amino acid residues that are essential for Fe(ii) binding. (B) Scheme to generate a series of germline-specific *Jmjd1a* and/or *Jmjd1b* knockout mice.

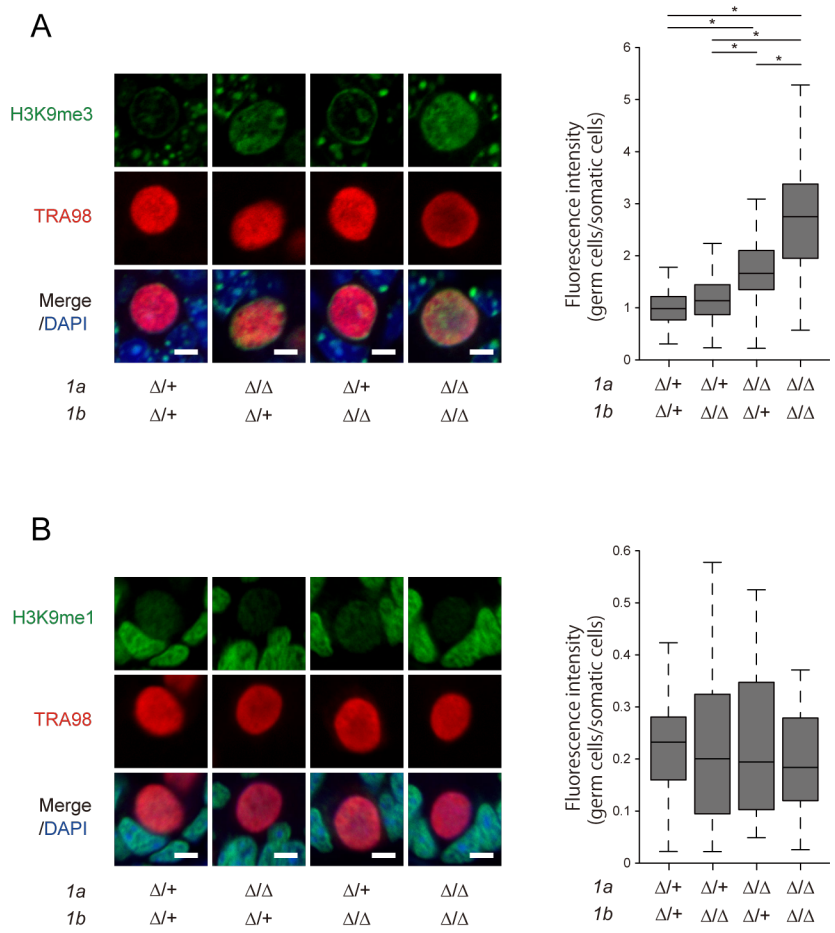

Supplementary Figure S2 (Related to Figure 2)
JMJD1A and JMJD1B Catalyze H3K9me3 Demethylation in Prospermatogonia

(A, B) Immunofluorescence analysis for H3K9me3 (A) and H3K9me1 (B) in P3 testes sections of the indicated genotypes. A TRA98 antibody was used to detect germ cells. Scale bars, 5 μm. Relative fluorescence intensity values were calculated by dividing the fluorescence intensities of germ cells by those of neighboring Sertoli cells (right panels). We examined >50 germ cells per genotype. *P < 0.05 (one-way ANOVA with Tukey's test).

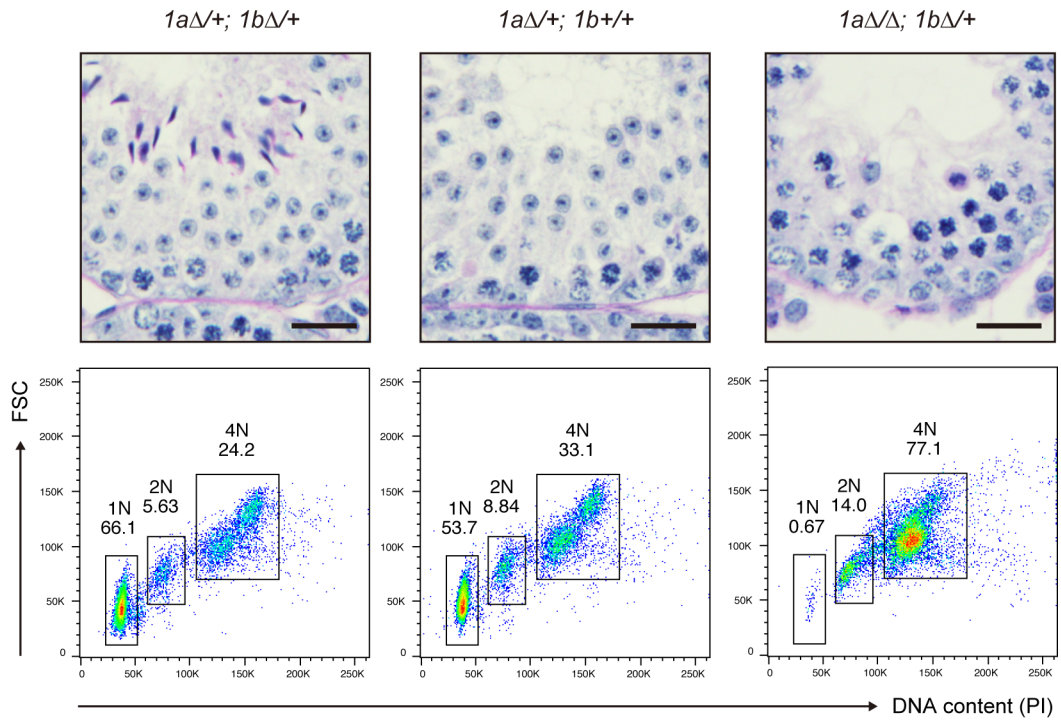

Supplementary Figure S3 (Related to Figure 3)

Role of JMJD1A and JMJD1B in meiotic progression. P28 testes sections of the indicated genotypes were stained with PAS-hematoxylin (top). Germ cells were dissociated from P28 testes of the indicated genotypes and then analyzed for DNA content (bottom). Briefly, testicular cells were fixed, stained with a TRA98 antibody and propidium iodide (PI), and then FACS sorted. Data show the DNA content of TRA98-sorted germ cells. Scale bars, 20 μm.

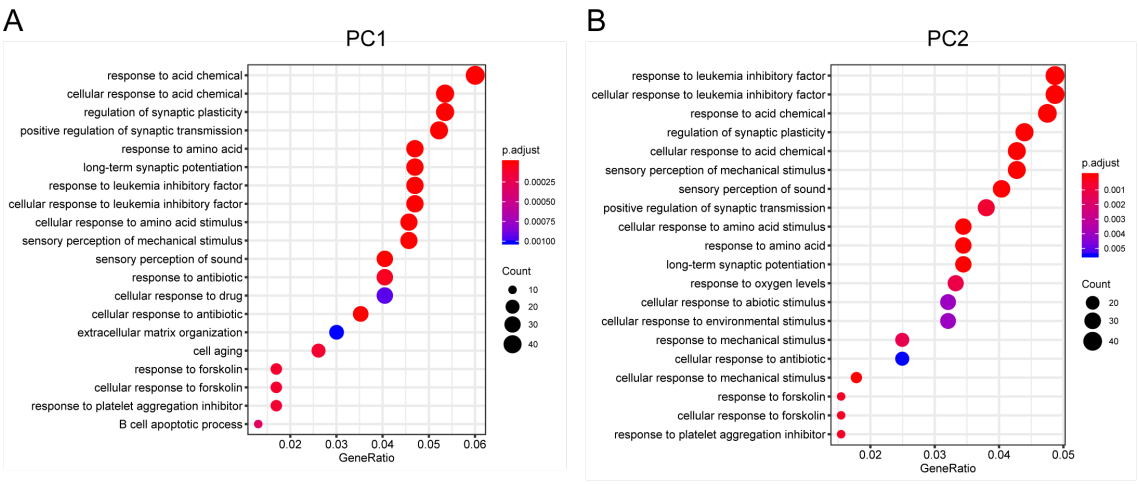

Supplementary Figure S4 (Related to Figure 4)

Gene Ontology analysis of genes contributing to PC1 and PC2 shown Fig. 4M. We calculated the loadings of PC1 and PC2 and used the top 5% of genes for Gene Ontology analysis.

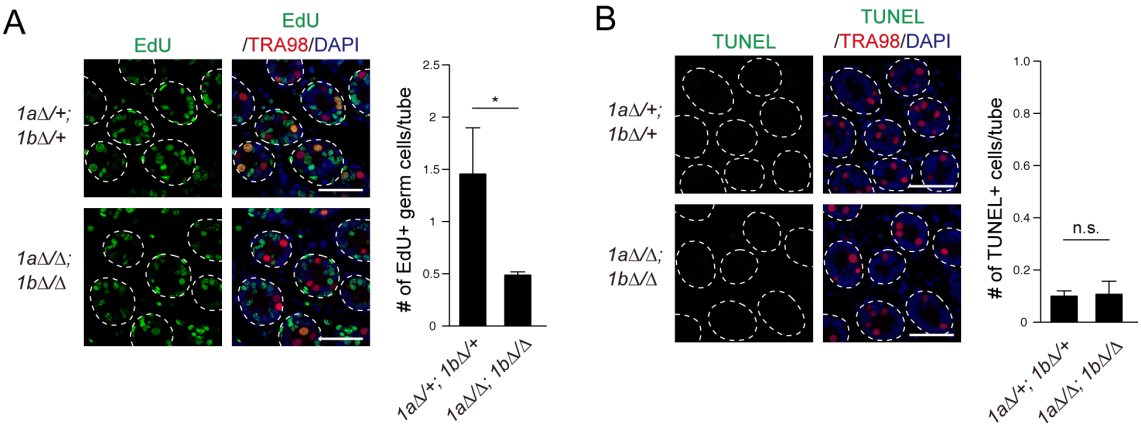

Supplementary Figure S5 (Related to Figure 5)

(A) Proliferation analysis of JMJD1A/JMJD1B-depleted germ cells at P3. Cells incorporating Edu were counterstained with a TRA98 antibody (left). Scale bars, 50 μm. Average numbers of EdU+ cells per cross-tubular section are summarized (right). Error bars represent ± SEM (n=3 mice each) *P < 0.05 (t-test). (B) Detection of apoptotic cells in JMJD1A/JMJD1B-depleted germ cells at P3. TUNEL-stained section of P7 testis of the indicated genotypes were counterstained with a TRA98 antibody (left). Scale bars, 50 μm. Average numbers of TUNEL+ cells per cross-tubular section are summarized (right). Error bars represent ± SEM (n=3 mice each); n.s., not significant (P>0.05, t-test).

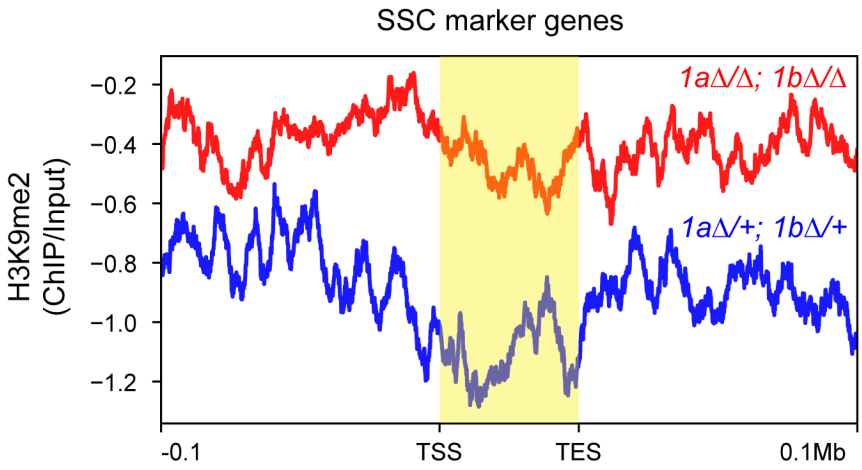

Supplementary Figure S6 (Related to Figure 6)

Distribution profile of H3K9me2 on SSC marker genes shown in Fig. 5F. Averaged H3K9me2 levels of the gene bodies and adjacent 100 kb regions for *Id4*, *Epcam*, *Cd9*, *Etv5*, *Plzf*, *Sohlh2*, *Pou3f1*, *Kit*, *Ret*, *Lhx1*, *Cdh1*, *Lin28a*, *Gfra1*, *Bcl6b*, *Pou5f1*, *Nanos3*, and *Stra8* are presented. Log2-transformed ratio of ChIP/Input is shown.

SUPPLEMENTAL EXPERIMENTAL PROCEDURES

Genotyping

Genotyping of the Vasa-Cre Tg, *Jmjd1a*-deficient, and *Jmjd1b*-deficient mice was performed by standard PCR using Quick Taq HS Dyemix (Toyobo). The primers sets used were: 5′-ATTTGGGCCAGCTAAACATGCTTCATCG-3′ and 5′-CCTTCCAGGGCGCGAGTTGATAGC-3′ for *Vasa-Cre*, 5′-TCCTACCCAGTACAAGAGGGAGAGTGC-3′ and 5′-GGGAATTCCCACATAAACCATGACATTGGC-3′ for *Jmjd1a*^{2lox}, 5′-TCCTACCCAGTACAAGAGGGAGAGTGC-3′ and 5′-AGAACATGAGACCTTGGGGCCAAGG-3′ for *Jmjd1a*^{1lox}, 5′-GCACCAAGCACTGCCACGGAGCTGA-3′ and 5′-CATACACCATCACATTAACAGCGTCTGAC-3′ for *Jmjd1b*^{2lox}, 5′-GCACCAAGCACTGCCACGGAGCTGA-3′ and 5′-GCAGCCCAGGTTGGCCTCTATGATC-3′ for *Jmjd1b*^{1lox}, and 5′-GAAGAACATCATATACCACGCAGTG-3′ and 5′-GGAATGTGGCACCCTCGGCTTGAGT-3′ for *Jmjd1b*$^{Flag\text{-}KI}$.

Preparation of germ cells

Germ cells were isolated from testes of *Vasa-Cre; Jmj1a; Jmj1b* conditional knockout mice or *Oct4*-EGFP Tg mice by fluorescence-activated cell sorting. Testes of indicated genotypes were digested in Accutase (Nacalai) supplemented with 0.5 mg/ml DNaseI (Sigma) to obtain a single cell suspension. For the conditional knockout mice, suspended cells were incubated with an anti-EPCAM antibody followed by incubation with Alexa488-conjugated anti-rat IgG antibody. Just before analysis, 1 μg/ml propidium iodide was added and EPCAM + cells were sorted from the FSC^{high} population using a FACS Aria II flow cytometer (BD Biosciences). For *Oct4*-EGFP Tg mice, EGFP^{+} cells and EGFP^{-} cells were sorted as germ cells and somatic cells, respectively. The purity of the germ cells was checked by immunostaining with the anti-VASA antibody.

Histological analysis

Testes were fixed in Bouin’s solution, embedded in paraffin and sectioned at 4 μm. Sections were deparaffinized, rehydrated and then

stained with either hematoxylin-eosin or hematoxylin-periodic acid-Schiff (PAS).

Immunofluorescence analysis

Testes were fixed in 4% paraformaldehyde (PFA) for 12 h at 4°C. For immunohistological analysis, testes were embedded in OCT compound (Sakura Finetek) and cut into 8-μm-thick sections using a standard protocol. The sections were washed with PBS, and antigen-retrieved at 105°C for 5 min in 10 mM citric acid buffer (pH 6.0). For whole-mount immunostaining, segments of seminiferous tubules were dissected from testes, fixed in 4% PFA for 2 h and then permeabilized with PBS containing 0.5% Triton-X100 and 1% BSA for 20 min at RT. All sections were blocked with TBS containing 2% skimmed milk and 0.1% Triton X-100 for 1 h, and were then incubated with the primary antibodies overnight at 4°C, followed by incubation with Alexa Fluor dye-conjugated secondary antibodies for 1 h and counterstaining with DAPI (1 μg/ml). The sections were mounted in Vectashield (Vector) and analyzed by confocal scanning microscopy (LSM700, Carl Zeiss) using Zen 2011 imaging software (Carl Zeiss). Fluorescence intensity was measured using NIH ImageJ software.

Quantitative RT-PCR Analysis

Total RNA was purified using an AllPrep DNA/RNA Micro Kit (Qiagen). cDNA was synthesized with ReverTra Ace qPCR RT Master mix (Toyobo) according to manufacture's instructions. SYBR premix Ex Taq II (Takara) was used for quantitative PCR. The following primer sets were used. 5′-ACTCCAGAGGATCGGAAATATGGGACC-3′ and 5′-GGGAATTCCCACATAAACCATGACATTGGC-3′ for *Jmjd1a*, 5′-GGAGATGCTGATGAGGTGACCAAGC-3′ and 5′-GGATCTTCTCTGCATCCTTCGCTGC-3′ for *Jmjd1b*, and 5′-ATGAATACGGCTACAGCAACAGG-3′ and 5′-CTCTTGCTCAGTGTCCTTGCTG-3′ for *Gapdh*.

TUNEL assay

TdT-mediated UTP nick end labeling (TUNEL) was performed with immunostained sections using the In Situ Cell Death Detection Kit (Roche) according to manufacturer's instructions. Images were collected with an

LSM700 microscope (Zeiss). The number of TUNEL-positive cells in each seminiferous tubule was counted using Image J software. More than 50 tubular sections were analyzed per sample.

Cell proliferation assay

P3 or P7 pups of indicated genotypes were subcutaneously injected with 0.25 mg EdU (Sigma). Twelve hours after injection, testes were collected from the pups and immunofluorescence staining for TRA98 was performed as described above. After immunostaining, Edu was stained using a Click-it Plus Edu Imaging Kit (Thermo Fisher Scientific) according to the manufacturer's instructions. The percentage of Edu-positive cells among $TRA98^+$ cells was calculated using Image J software. More than 300 $TRA98^+$ cells were counted per sample.

FACS analysis

Testes were digested with Accutase (Nacalai) to obtain a single cell suspension. Suspended cells were fixed with 2% PFA in PBS for 10 min, permeabilized with ice-cold ethanol for 20 min, and blocked with 0.5% skimmed milk in PBS for 1 h. Cells were then stained with primary antibodies overnight at 4°C and subsequently incubated with Alexa Fluor Dye-conjugated secondary antibodies (Life Technologies) for 1 h at room temperature. For DNA content analysis, testicular cells were stained with TRA98 antibody using the above protocol and were then incubated with RNase and PI just before analysis. Data were collected using a FACS Aria II (BD Bioscience) and analyzed with FlowJo software (TreeStar).

Immunoblot analysis

Whole lysates of germ cells and somatic cells were fractionated by SDS electrophoresis and transferred to nitrocellulose membranes. Proteins on the membranes were visualized using an enhanced chemiluminescence (ECL) kit (Perkin Elmer).

RNA sequence analysis

Total RNA was extracted using an All Prep DNA/RNA Micro Kit (Qiagen). cDNA libraries were prepared from total RNA using a TruSeq Stranded mRNA LT Sample Prep Kit (Illumina). Quality control was performed using a

Bioanalyzer (Agilent). The libraries were sequenced on an Illumina Hiseq 1500 or 2000. Sequence reads were mapped to the mouse mm10 genome using TopHat2 (v2.1.1) with default parameters. Fragments Per Kilobase of transcript per Million mapped reads (FPKM) were estimated using Cufflinks (v2.1.1). Differentially expressed genes between P0 and P3 or P7 germ cells were calculated using Cuffdiff. PCA analysis and Gene Ontology analysis were performed using R statistical software (v3.5.1). PC loadings were calculated using the prcomp() function. Gene Ontology analyses were performed with the enrichGO() function in the clusterProfiler package. Heatmaps were visualized using the Heatmap() function in the ComplexHeatmap package.

ChIP-seq analysis

ChIP of H3K9me2 was performed following a previously described protocol (Tachibana et al., 2008) with slight modification. Briefly, 0.7 x 10^5 cells were suspended in 25 µl 0.3 M sucrose-containing buffer 1 (60 mM KCl, 15 mM NaCl, 5 mM $MgCl_2$, 0.1 mM EGTA, 0.5 mM DTT, 15 mM Tris-HCl pH 7.5, and protease inhibitor cocktail). The cells were then lysed on ice for 10 min by the addition of 25 µl 0.8% NP40. Four hundred microliters of 1.2 M sucrose-containing buffer 1 were then added and the chromatin was pelleted by centrifugation. The pellets were digested with micrococcal nuclease (0.05 U, Takara) in 10 µl digestion buffer (0.32 M sucrose, 4 mM $MgCl_2$, 1 mM $CaCl_2$, 50 mM Tris-HCl pH 7.5) by vortexing at 37°C for 15 min. Digestion was then stopped with EDTA. After centrifugation the supernatant was incubated with anti-H3K9me2-conjugated magnetic beads (Dynabeads Protein G, Invitrogen) in 50 µl incubation buffer (50 mM NaCl, 5 mM EDTA, 0.1% NP40, 20 mM Tris-HCl pH 7.5) at 4°C for 6 h. Then, DNA was extracted from the immune complex according to the standard protocol. DNA from input and ChIP fractions was processed using a SMARTer ThruPLEX DNA-seq Kit (TaKaRa) and sequenced using the Illumina HiSeq 1500 system according to the manufacturer's instructions. In brief, the DNA was end-repaired, ligated to sequencing adapters, amplified, and sequenced to generate single-end reads. Sequence reads were mapped to the mouse mm10 genome using Bowtie2 (v 2.1.0) with default parameters. Only uniquely mapped and non-redundant reads were used for further analysis. DROMPA software (v 3.2.6) (Nakato et al., 2013) was used for

processing the mapped reads and calculating gene density in the mouse mm10 genome. For visualizing H3K9me2 profiles across chromosome 5, the reads were processed using the PC_ENRICH command (with the -binsize 500000 -outputwig 1 -owtype 2 option, to output the normalized read density of ChIP and the corresponding input samples). The processed H3K9me2 profiles and the gene density were visualized using the plot() function in R or Integrated Genome Viewer (IGV). Plotting of averaged reads around gene bodies was performed using the bamCompare, computeMatrix, and plotProfile commands in DeepTools (v.3.2.1). The parameters for Fig. 6H and S6 are as follows: Fig.6H, bamCompare (-bs 100 --smoothLength 200 --operation ratio --ignoreDuplicates), computeMatrix (--beforeRegionStartLength 3000 --regionBodyLength 5000 --afterRegionStartLength 3000 --skipZeros), plotProfile (--perGroup); FigS6, bamCompare (-bs 1000 --smoothLength 5000 --operation log2 --ignoreDuplicates), computeMatrix (--beforeRegionStartLength 100000 --regionBodyLength 50000 --afterRegionStartLength 100000 --skipZeros), plotProfile (--perGroup).

SUPPLEMENTAL REFERENCES

Nakato, R., Itoh, T., and Shirahige, K. (2013). DROMPA: easy-to-handle peak calling and visualization software for the computational analysis and validation of ChIP-seq data. Genes Cells *18*, 589-601.

Tachibana, M., Matsumura, Y., Fukuda, M., Kimura, H., and Shinkai, Y. (2008). G9a/GLP complexes independently mediate H3K9 and DNA methylation to silence transcription. The EMBO journal *27*, 2681-2690.